Cenozoic extension in the Kenya Rift from low-temperature thermochronology: Links to diachronous spatiotemporal evolution of rifting in East Africa

Verónica Torres Acosta*[1], Alejandro Bande[1], Edward R. Sobel[1], Mauricio Parra[2], Taylor F. Schildgen[1,3], Finlay Stuart[4], Manfred R. Strecker[1]

[1] *Institut für Erd- und Umweltwissenschaften, Universität Potsdam, Karl-Liebknecht-Str. 24, 14476 Potsdam, Germany.*

[2] *Instituto de Energia e Ambiente (IEE). Universidade de São Paulo (USP). São Paulo, SP, Brazil.*

[3] *Deutsches GeoForschungsZentrum (GFZ) Potsdam, Potsdam, Germany*

[4] *SUERC, Rankine Avenue, Scottish Enterprise Technology Park, East Kilbride, G750QF, Scotland, UK*

***** Corresponding author, e-mail: acosta@geo.uni-potsdam.de

Key points:

- **Data and modeling show Paleogene and middle Miocene cooling episodes**
- **Cooling episodes separated by stable conditions, slow exhumation or subsidence**
- **Extension pattern is compatible with random rift initiation above a plume**

This article has been accepted for publication and undergone full peer review but has not been through the copyediting, typesetting, pagination and proofreading process which may lead to differences between this version and the Version of Record. Please cite this article as doi: 10.1002/2015TC003949

Abstract

The cooling history of rift shoulders and the subsidence history of rift basins are cornerstones for reconstructing the morphotectonic evolution of extensional geodynamic provinces, assessing their role in paleoenvironmental changes, and evaluating the resource potential of their basin fills. Our apatite fission-track and zircon (U-Th)/He data from the Samburu Hills and the Elgeyo Escarpment in the northern and central sectors of the Kenya Rift indicate a broadly consistent thermal evolution of both regions. Results of thermal modeling support a three-phased thermal history since the early Paleocene. The first phase (~65-50 Ma) was characterized by rapid cooling of the rift shoulders and may be coeval with faulting and sedimentation in the Anza Rift basin, now located in the subsurface of the Turkana depression and areas to the east in northern Kenya. In the second phase, very slow cooling or slight reheating occurred between ~45 and 15 Ma as a result of either stable surface conditions, very slow exhumation, or subsidence. The third phase comprised renewed rapid cooling starting at ~15 Ma. This final cooling represents the most recent stage of rifting, which followed widespread flood-phonolite emplacement and has shaped the present-day landscape through rift shoulder uplift, faulting, basin filling, protracted volcanism, and erosion. When compared with thermochronologic and geologic data from other sectors of the East African Rift System, extension appears to be diachronous, spatially disparate, and partly overlapping, likely driven by interactions between mantle-driven processes and crustal heterogeneities, rather than the previously suggested north-south migrating influence of a mantle plume.

1. Introduction

Continental rift systems are first-order tectonic features that record the early stages of continental break-up. In magmatically controlled rifts, long-wavelength crustal updoming and

the development of dynamic topography prior to the onset of volcanism and normal faulting underscore the role of mantle-driven, thermally controlled processes in the evolution of these regions [e.g., *Crough*, 1983; *Ebinger and Sleep*, 1998; *Moucha and Forte*, 2011]. In the East African Rift System (EARS), such changes in topography and relief have had far-reaching consequences, including impacts on atmospheric circulation patterns that in turn affect rainfall patterns, drainage systems, and surface processes [e.g, *Levin et al*. 2009; *Sepulchre et al*., 2006; *Ebinger and Scholz*, 2012; *Wichura et al.*, 2010; 2015]. In addition, the interplay between extensional tectonics and superposed changes in climate has given rise to gateways and migration corridors for hominids and other mammals, thus fostering speciation [*Bobe and Behrensmeyer*, 2004; *Bailey and King*, 2011; *Bailey et al.*, 2011].

Uplift, volcanism, and normal faulting in the EARS are hallmarks of one of the largest magmatic extensional zones on Earth [*Burke*, 1996]. Comprised of the largely amagmatic western and the magmatic eastern branch, the ~5000-km-long EARS has generated a series of transiently linked and isolated rift basins [*Tiercelin and Lezzar*, 2002; *Ebinger and Scholz*, 2012]. The areally extensive mantle anomaly that underlies the EARS [e.g., *Simiyu and Keller*, 1997; *Ebinger and Sleep*, 1998; *Achauer and Masson*, 2002] helps support average elevations of ~1000 m [*Moucha and Forte*, 2011]. As such, understanding the mechanisms of rifting and its spatiotemporal evolution are critical for exploring how geodynamic and surface processes are potentially linked with topographic development, magmatic evolution, and long-term environmental and biotic impacts in rift systems. Changes in each of these aspects over time throughout the EARS have been difficult to quantify, but valuable information has been obtained from the sedimentary and volcanic rift-basin strata [e.g., *Frostick and Reid*, 1990; *Morley et al.*, 1992; *Pickford and Senut*, 1994; *Renaut et al.*, 1999; *Odada and Olago*, 2002; *Saneyoshi et al.*, 2006; *Ebinger and Scholz*, 2012; *Tiercelin et al.*, 2012; *Roberts et al.*, 2012]. Unfortunately, many of the rift basins do not allow for a direct inspection of such

deposits, because old strata either lie below thick volcano-sedimentary sequences or areally extensive lakes [e.g., *Flannery and Rosendahl*, 1990; *Cohen et al.*, 1993; *Scholz et al*., 1994; *Hautot et al.*, 2000], or because differential faulting, uplift, and erosion along the rift flanks have been insufficient to expose such deposits. For these reasons, many studies of the spatiotemporal trends in rift-basin formation have relied on the combined analysis of geophysical data, field observations, and isolated drill-core data.

Low-temperature thermochronometry, such as apatite fission-track and apatite and zircon (U-Th)/He dating, combined with thermal history modeling, constitute powerful alternative tools to investigate cooling as a proxy for tectono-thermal and climate-driven erosion processes in rift settings [*Fitzgerald*, 1992; *Foster and Gleadow*; 1992; 1996; *van der Beek et al.*, 1998]. Thermochronology studies have been carried out throughout the EARS aimed at unraveling the history of basin formation, rift-shoulder exhumation, and different tectono-thermal episodes associated with mantle-plume activity. These studies have addressed the tectonic evolution of the western branch of the EARS in the Rwenzori Mountains [*Bauer et al*., 2010; 2012] and the Malawi and Rukwa rifts [*van der Beek et al.*, 1998; *Roberts et al.*, 2012], and the evolution of the eastern branch in Ethiopia [*Pik*, 2008], northern Tanzania [*Noble et al., 1997; Mbede*, 2001], and Kenya [*Wagner*, 1992; *Foster and Gleadow*, 1992; 1996; *Spiegel et al*. 2007]. In the greater Turkana region and the western rift-shoulder areas of northern Kenya (Fig. 1), these investigations have provided helpful constraints on the regional onset of Mesozoic and early Cenozoic rifting [*Foster and Gleadow*, 1996; *Spiegel et al.*, 2007]. However, the spatial extent of the related tectono-thermal events, the formation of older rift basins underlying the late Cenozoic rifts, and the role of their structures in influencing Miocene to Recent rifting is unclear.

The onset of rifting in East Africa has been associated with a southward-directed migration of volcanism, which in turn has been inferred to be linked with the northward

motion of the African plate over a mantle plume [*Ebinger and Sleep*, 1998; *Nyblade and Brazier*, 2002]. Accordingly, the onset of tectonic activity in the eastern branch of the rift is also thought to have followed this temporal trend from Ethiopia to northern Tanzania [*Nyblade and Brazier*, 2002]. In contrast, *Zeyen et al.* [1997] proposed that the onset of extension was less systematic, and largely dictated by the spatially variable mechanical properties of the lithosphere and crust. The notion that rifting and volcanism did not follow a systematic, southward migration has been recently emphasized again by numerical modeling [*Koptev et al.*, 2015] and by a synopsis of the age of volcanism in the different sectors of the EARS, from which a synchronous onset of volcanic activity in East Africa has been proposed [*Michon*, 2015]. Furthermore, studies of noble gases in East African lavas and xenoliths suggest the existence of separate plume heads in Ethiopia and Kenya [*Halldórsson et al.*, 2014]. As the Kenya Rift is located between the Tanzania and Turkana-southern Ethiopia extensional provinces, it constitutes an important link between different extensional sectors in the volcanically active eastern branch of the EARS and is thus in a crucial location to further test these ideas.

Here we report 15 apatite (U-Th)/He (AHe), 13 apatite fission-track (AFT), and 5 zircon (U-Th)/He (ZHe) ages from basement rocks that were collected along three elevation transects at the Elgeyo escarpment and the Samburu Hills (Nyiru Range) on the eastern and western rift shoulders and steep rift flanks of basins in northern Kenya (Figs. 1 and 2). Following thermal modeling of our data using the HeFTy [*Ketcham*, 2005; *Ketcham et al.*, 2009] and QTQt software programs [*Gallagher*, 2009; *Gallagher*, 2012], we use the cooling histories to help elucidate the Cenozoic tectono-thermal evolution of the Kenya Rift shoulders and its implications for the overall structural evolution of the EARS.

2. Geological setting and tectonic history

In Kenya, the EARS is characterized by asymmetric rift basins, central volcanoes, and high rift shoulders (up to ca. 2000 masl in western Kenya) bounded by escarpments where late Proterozoic crystalline basement rocks are exposed [*Maboko*, 1985; *Smith*, 1994; *Smith and Mosley*, 1993; *Shackleton*, 1993]. Our study area comprises the eastern shoulders of the northern Kenya Rift and the transition between the northern and central Kenya rifts along the western rift margin (Fig. 1).

Geophysical data, stratigraphic information, and dated volcanic lava flows have furnished information on the early rifting history in northern Kenya, which began during the late Mesozoic [*Foster and Gleadow*, 1992; 1996; *Morley et al.*, 1992; *Wagner et al*. 1992; *Ebinger*, 2000; *Tiercelin et al.*, 2004; 2012]. These early episodes of extension affected areas between the Indian Ocean and the Lake Turkana region, leading to the accumulation of thick lacustrine, fluvial, and eolian strata in the NW-SE oriented Cretaceous Anza Rift (Fig. 1). In its central part, the buried Anza Rift was active during the late Cretaceous, whereas it continued to be active into the late Tertiary in the northern Lamu Embayment (Fig. 1), in the vicinity of the present-day coast of the Indian Ocean [*Bosworth and Morley*, 1994]. Farther west, the Anza Rift is inferred to transition into the eastern sectors of the Cretaceous Central African Rift Zone [*Schull*, 1988].

Subsequent Cenozoic extension in northern Kenya is recorded in the Turkana-Lokichar rift zone (Fig. 1b), but was preceded by volcanism at about 35 Ma, followed by Oligocene normal faulting and the formation of several halfgraben basins [*Morley et al*., 1992]. These basins span the region between the Ugandan border and Lake Turkana (Fig. 1), and they host sedimentary fills 5 to 8 km thick that include intercalated volcanic rocks [*Morley et al*., 1992; *Tiercelin et al.*, 2012]. However, apatite (U-Th)/He and fission-track data from the western rift flank (Cherangani Hills of northern Kenya) and from the present-day eastern rift flank southeast of Lake Turkana (Figs. 1 and 2) only reveal clear episodes of

cooling during the late Cretaceous to Paleocene and during the late Neogene [*Foster and Gleadow, 1996; Spiegel et al.*, 2007].

Today, the northern Kenya Rift encompasses the wide, early Cenozoic Turkana-Lokichar rift zone, but the Miocene to Recent manifestations of rifting are primarily located in the eastern sector of this extensional province, between approximately 1° and 4.5°N latitude. This region is characterized by the active, down-to-the-east halfgraben basin of the NNE-oriented Suguta Valley [*Bosworth and Maurin*, 1993; *Saneyoshi et al*., 2006; *Melnick et al*., 2012] and the northern sector of the NNE-oriented Elgeyo Escarpment farther west (Fig. 1b). The rift floor in the Suguta Valley is at ~300 masl, whereas the antithetically faulted monocline on the eastern rift margin has an average elevation of ~1400 masl [*Bosworth and Maurin*, 1993]. There, the rift shoulder exposes gneissic Precambrian basement in the Samburu Hills, our first study site, which locally reach up to 1900 masl (Figs. 1 and 2). To the north of the Suguta Valley is the active Kino Sogo rift zone; this extensional sector transitions northward into the Chew Bahir Rift of southern Ethiopia, which is an integral part of the Main Ethiopian Rift (Fig. 1).

The Elgeyo Escarpment, our second study site, is located along the western margin of the northern Kenya Rift and the northernmost sector of the NNW-oriented central Kenya Rift, where the escarpment transitions southward into the Mau Escarpment (Fig. 1b). The Elgeyo Escarpment is one of the most prominent fault-line escarpments of the Kenya Rift. In its southern sector, the escarpment is ~900 m higher than the adjacent Kerio sedimentary basin (Fig. 2). The Elgeyo Escarpment is related to a down-to-the-east normal fault, which exposes steeply eastward-dipping Proterozoic gneisses of the pan-African orogeny [*Chapman et al., 1978*; *Maboko*, 1985; *Hetzel and Strecker*, 1994]. The Cenozoic faults along the Elgeyo Escarpment follow the gneissic foliation and change in strike where the foliation is cut by NW-striking Proterozoic dextral shear zones [*Strecker et al.*, 1990; *Shackleton*, 1993]. These

reactivated shear zones influence the geometry and areal distribution of strata of the Kerio sedimentary basin [*Mugisha et al.*, 1997]. The basement shear zones are overlain by arkosic sandstones, conglomerates and lacustrine shales of unknown age, and up to 150-m-thick, 14-m.y.-old phonolites [*Lippard*, 1973; *Ego*, 1994; Supplementary Figure 1] that also cap the western rift shoulder. Faulting along the Elgeyo Escarpment in this sector postdates the emplacement of the middle Miocene phonolite flows and generated the westward-tilted Kamasia fault block to the east (Fig. 2), which in turn is delimited by a major down-to-the-east normal fault to the east [e.g., *Chapman et al.*, 1978]. The Kamasia Range thus forms the barrier between the Kerio Basin and the Baringo Basin farther east, which now hosts the active volcano-tectonic axis of this part of the Kenya Rift.

3. Methodology

We constrain the Cenozoic cooling of the Precambrian Mozambique Belt gneisses exposed on the western and eastern rift shoulders of the northern Kenya Rift and the northernmost sector of the central Kenya Rift using apatite fission-track thermochronology (AFT; apatite partial annealing zone, PAZ, ~60-~120°), apatite (U-Th-Sm)/He thermochronology (AHe, partial retention zone, APRZ ~40°-85°C) and zircon (U-Th)/He thermochronology (ZHe; ZPRZ ~120-~200°C (assuming that zircons remained in this temperature range for about 90 Myr [e.g. *Reiners and Brandon*, 2006; *Wolf et al*., 1998; *Ketcham et al.*, 1999; *Reiners*, 2005]). We collected seven samples (KN83 through KN89) along a W-E oriented profile between 1300 and 1900 masl in the Samburu Hills (SH), on the eastern rift flank (Fig. 3, Tables 1, 2 and Supplementary table 1). On the western flank, we collected one steep profile across the northern Elgeyo Escarpment (NEE) and one across the southern Elgeyo Escarpment (SEE) (Fig. 2). The NEE profile comprises six samples (KN97 through KN102) collected between 1280 and 1850 masl, and the SEE profile comprises five

samples (KN53, KN55, KN91, KN92, KN94) collected between 1350 and 1780 masl. The Elgeyo escarpment profiles are separated by ca. 50 km and were collected perpendicular to the main fault-line escarpment (Fig. 2). In addition, sample KN50 was collected between the two profiles and analyzed for AFT, although it was not used to help constrain the thermal modeling.

Mineral separation and sample preparation for AFT, AHe, and ZHe analyses followed standard procedures [e.g. *Dobson, 2006*] and are briefly described below. Eighteen samples yielded enough apatite for AFT and AHe analysis, and six samples were analyzed with the ZHe method.

3.1. Apatite fission-track analysis

AFT samples were analyzed with a Leica DMRM microscope at the University of Potsdam. Approximately 20 good-quality grains per sample were randomly selected and dated using the external detector method and the zeta calibration technique [*Hurford*, 1983] (see Table 1.). The pooled age is reported (±1σ) when samples pass the Chi-squared test ($P(\chi^2) \geq 5\%$) [*Galbraith*, 1981]; for KN50, the central age is reported because the sample failed this test. We also report confined track-length distributions of seven AFT samples (see details in Table 1). ^{252}Cf irradiations were performed (see Supplementary material) to obtain a larger number of horizontally confined tracks for track-length measurements [e.g. *Donelick et al*, 2005]. The angle between the confined tracks and the crystallographic c-axes was routinely measured. The size of the etch-pit diameter parallel to the c-axis (Dpar) was also determined, as it is a kinetic parameter used in thermal history modeling [*Donelick et al.*, 1999; *Ketcham et al.*, 1999] At least four Dpar values were measured per crystal; the data were corrected following *Sobel and Seward* [2010].

3.2. Apatite (U-Th-Sm)/He analysis

The AHe method is based on the accumulation of alpha particles produced by U, Th and Sm series decay [*Ehlers and Farley*, 2003]. Ages are corrected for alpha ejection near the margins of the crystal assuming a homogenous distribution of U, Th, and Sm [*Farley et al.*, 1996; *Ehlers and Farley*, 2003]. Samples were analyzed at the Scottish Universities Environmental Research Center (SUERC) following the procedure described by *Foeken et al.* [2006]. We analyzed between 1 and 3 apatite crystals of similar radius per sample (Supplementary Table 1). Corrections for He recoil loss were made following the procedures of *Farley and Stockli* [2002]. The correction factor (Ft) was calculated based on the retention and stopping distance of the alpha particle in the crystal and the size of each grain analyzed. The reproducibility of the ^{3}He spike was determined from three daily measurements against an accurately known ^{4}He standard. Standard ^{4}He abundance measurements have within–run precision of better than 0.1% (1σ) and between-run precision of 0.2% (1σ) [*Persano et al.*, 2002].

U, Th and Sm analyses were performed on a VG plasma Quad PQ2+ICP-MS. After ^{4}He analysis, each crystal was dissolved and spiked with ~0.45 ng ^{230}Th and 0.20 ng ^{235}U with approximately 2 ml of HNO_3. Total analytical uncertainty on all ages was approximately 1-3% (1σ), which is dominated by the uncertainty in the U and Th spike concentrations [e.g., *Dobson*, 2006; *Foeken et al.*, 2006], He determinations, blank corrections, and uncertainties on grain-size measurements for α-correction.

3.3. Zircon (U-Th)/He analysis

The (U-Th)/He analysis of zircons is also based on the accumulation and diffusion of alpha particles produced by the decay of U and Th. After mineral-separation at the University of Potsdam, we used the facilities at SUERC following analytical procedures described by

Foeken et al. [2006] and *Dobson* [2006]. Seven samples with 1 to 3 single-crystal aliquots each were analyzed. With respect to the Ft correction, we followed procedures described in *Farley and Stockli* [2002], and we again assumed a uniform distribution of U and Th. Total analytical uncertainty is dominated by the uncertainty in the U and Th spike concentrations [*Dobson*, 2006; *Foeken et al.*, 2006], He determinations, and blank corrections.

3.4. Age-elevation relationships (AERs) and thermal history modeling

The relationship between thermochronologic ages and elevations of different samples along an elevation profile are commonly used to determine rates and amounts of exhumation [e.g., *Dobson et al.*, 2009; *Foeken et al.*, 2006]. However, the thermal structure of the uppermost crust could be influenced by topography, erosion, faulting, and advection [e.g., *Ehlers and Farley*, 2003; *Gallagher*, 2005], which complicate direct interpretations of the slope of age-elevation plots [e.g., *Valla et al.*, 2010; *van der Beek et al.*, 2010].

To determine the Cenozoic cooling history recorded by samples within our age-elevation profiles, we used two different thermal modeling approaches. We performed forward and inverse Monte Carlo modeling of time-temperature paths combining AFT and ZHe data using the HeFTy 1.8.2 software [*Ketcham*, 2005] for individual samples, and we used the QTQt software [*Gallagher et al.* 2009; *Gallagher*, 2012] to derive integrated cooling constraints from multiple samples within an age-elevation transect. AHe data were not used for modeling due to the high dispersion of single-grain ages, as discussed in section 4.

The HeFTy program is effective for assessing the thermal history of a single sample. The output reflects the goodness of fit of the models, which allows for testing different cooling histories. However, the program has not yet been adapted for modeling multiple samples within an elevation profile. In contrast, the QTQt program is well suited for the latter task. Therefore, we use the HeFTy results to determine approximate constraints that can be

applied during QTQt modeling of the complete profile.

To resolve the Cenozoic thermal history of the rocks along each profile, we tested two contrasting thermal history scenarios: monotonic cooling versus Neogene reheating and cooling. We used the HeFTy and QTQt programs to predict time-temperature paths for these two scenarios that are consistent with our AFT age and track-length distribution data and our ZHe ages. Additionally, we used geological constraints, such as the initiation of volcanism north of the study area [*Morley et al.*, 1992; *Ebinger and Sleep*, 1998], to provide some brackets on possible cooling paths.

4. Results

4.1. Apatite fission-track dating results

The apatite fission-track cooling ages are shown in Table 1. Over the 400-m elevation range of the Samburu profile (SH), samples KN89, KN85, and KN83 yielded ages ranging from 39.4 ± 3.0 Ma to 50.3 ± 8.0 Ma. Although the elevation difference is small, this section provides the best relief and outcrop conditions in the area. Mean track lengths from samples KN83 and KN85 are 12.2 and 11.9 μm, respectively; sample KN89 did not yield a meaningful number of track lengths (n=2, Table 1). Samples from the northern Elgeyo transect (NEE, 4 samples) yielded ages ranging from 26.2 ± 3.0 Ma to 38.8± 3.0 Ma, with mean track lengths of 11.2 to 11.8 μm that were measured from 3 out of the 4 samples (KN99, KN100, and KN102).

The southern Elgeyo transect comprises six samples with an age range between 4.6 ± 1.0 Ma and 9.2 ± 2.0 Ma. No confined track lengths were found in those samples. In comparison to the AFT ages of the NEE and SH profiles, the young AFT ages of this transect together with the lack of a clear increase in age with elevation may be related to reheating as a result of nearby fluorite mineralization associated with the emplacement of Miocene lava

flows. The fluorite mineralization shows ENE to E-trending growth fibers in the plane of the steeply E-dipping foliation [*Aljabri*, 1992; *Hetzel and Strecker*, 1994; *Ogola et al*., 1994]. As fluorite mineralization involves temperatures between 120 and 260°C [e.g., *Richardson and Holland*, 1979], AFT ages were likely at least partially reset, and therefore we do not use those data to model the tectono-thermal history in this part of the study area.

4.2. Apatite (U-Th-Sm)/He results

We report 54 single-grain AHe ages from 15 samples (Supplementary Table 1). In most samples, several single-grain AHe ages are older than the AFT age from the same sample, and only a few aliquots yield younger AHe ages (Supplementary Table 1, Fig. 3). With respect to calibration and operation of the analytical machines, Ft corrections on potential non-ideal geometries, and grain-size measurement uncertainties, none can explain independently the dispersion of the data. Below we consider other possibilities.

Because prominent zonation in U and Th can also affect AHe ages, we examined the distribution of induced tracks in the micas of AFT samples that were also analyzed with the AHe method to assess the variability of the U distribution within single grains. Many of the samples contained numerous grains with pronounced U zoning, often with U-rich rims, although U-rich cores relative to the rims are required to explain ages that appear too old. Two samples (KN53, KN55) were also characterized by very high crystal-dislocation densities. During AFT analysis, such crystals were not analyzed. However, these characteristics can help explain the high age dispersion within the AHe data.

Particularly in the case of slowly cooled apatites, differing amounts of radiation damage reflected by variable effective uranium ("eU") have been invoked to explain widely dispersed AHe ages [e.g., *Flowers*, 2009] or AHe ages that are older than AFT ages [e.g., *Green et al.*, 2006; *Hansen and Reiners*, 2006, *Gautheron et al.*, 2009]. Higher eU in apatite

leads to more radiation damage, higher He retentivity, and hence a higher effective closure temperature and a greater accumulation of He for a given cooling history [*Flowers et al.*, 2007]. Alternatively, variations in the effective diffusion domain size could influence the closure temperature of the crystal [*Gautheron et al.*, 2009]. To explore these possibilities, we plotted AHe age versus eU and versus grain size. However, the ages do not show a clear correlation with either parameter (Supplementary Fig. 2).

Radiation damage and variable eU problems are commonly discussed in cases with AHe ages that are much older (>100 Ma) [e.g. *Flowers*, 2009] than those in this study. However, prolonged residence time at a low temperature (i.e. ~80-100°C) prior to late burial heating has been shown to exert a strong influence on ^{4}He retentivity and hence on the effective closure temperature [*Fox and Schuster*, 2014]. In our study, the basement rocks are ~500-m.y.-old and are related to the Panafrican orogeny [*Maboko*, 1985; *Smith*, 1994]. Between these early tectonic processes and the initiation of Cenozoic rifting [e.g.*Foster and Gleadow*, 1996; *Spiegel et al.*, 2007], the samples remained at a relatively constant position below the surface (~3 km). This thermal history is quite analogous to the Grand Canyon [*Fox and Schuster*, 2014], suggesting that AHe results from there are applicable to our study. The extremely long residence time of samples at depths of a few km led to a variable and large amount of accumulated radiation damage, which caused higher ^{4}He retentivity and hence anomalously old AHe ages. Such a scenario provides a better explanation for the old ages in our study than variations in grain size, eU, zonation, or analytical problems.

4.3. Zircon (U-Th)/He results

We analyzed a subset of samples from each of our three elevation profiles for ZHe. From the Samburu Hills profile, we analyzed samples KN85 and KN83. Two aliquots from sample KN85 provide a ZHe mean age of 50.6 ± 5.2 Ma. From sample KN83, the

anomalously young age (1.5 Ma) is paired with very low He and high U and Th concentrations. Induced tracks in the external detector from occasional zircons included in the AFT grain mount of the same sample show that many of these zircons are strongly zoned and have U-rich rims. Therefore, data from this sample was not plotted in the age-elevation plot and not used for thermal modeling (Fig. 3a). From the Northern Elgeyo Escarpment profile, samples KN97 and KN102 yielded ZHe ages of 59.7 ± 6.1 Ma (single aliquot) and mean age of 55.9 ± 5.6 Ma (three aliquots), respectively. A fourth aliquot of sample KN102 was discarded due to the low reproducibility of the age (Table 2). From the Southern Elgeyo Escarpment profile, samples KN91, KN92, and KN94 (Fig. 3c) have mean ages of 53.9 ± 5.5 Ma (two aliquots), 42.2 ± 4.3 Ma (two aliquots), and 56.7 ± 5.8 Ma (three aliquots), respectively.

4.4. Thermal history modeling of elevation transects

We performed thermal modeling on the NEE and SH transects. Thermal models that incorporated the AHe data were incompatible with the AFT data. Because of the large AHe age dispersion, low reproducibility of ages, and strongly likelihood of variable ^{4}He retentivity (as discussed previously), we decided to base the thermal modeling and our interpretations on only the AFT and ZHe data. (See Supplementary Table 1 and Supplementary Figure 2).

Our general approach was to first model an individual sample from an elevation profile (sample KN85 from profile SH, elevation 1600 m, and sample KN102 from profile NEE, elevation 1852 m, Fig. 3) using the HeFTy program. The HeFTy modeling results were used as the basis for defining a common thermal history of the samples [e.g. *Prenzel et al.* 2013] along the vertical profile. Next, we used QTQt to model the 3 samples from the SH profile simultaneously and the 4 samples from the NEE profile simultaneously. Monotonic cooling and reheating paths were tested with both programs. Constraint boxes were first

defined to observe preferential cooling paths of the analyzed samples. In subsequent runs, the constraint boxes were shifted to examine the reliability of inflection points representing changes in modeled cooling rates and to allow for reheating.

Input parameters for modeling included AFT data (age, c-axis non-projected track lengths, and Dpar values), the ZHe data, and present-day surface temperatures. Acceptable-fit paths (goodness of fit >0.05) from the HeFTy models of individual samples were considered for interpretation.

4.4.1. Thermal modeling of data from the Samburu Hills

For our thermal modeling of the Samburu Hills (SH) data, we first ran models with monotonic cooling paths using both the HeFTy and QTQt programs (Figs. 4a and 4b). We defined a first constraint box with a temperature range from 135 to 15°C for HeFTy (Fig. 4a) and for QTQt (Fig. 4b) over a time range from 15 Ma to the present. Second constraint boxes were defined between ~130 and 30°C at ~30 to 20 Ma. Third constraint boxes were defined between 230 and 160°C at ~75 to 45 Ma to be compatible with the AFT and ZHe cooling ages. HeFTy models always end with a temperature constraint at the present-day ranging from 25 to 15°C. The QTQt models end at present-day temperatures from 0° to 50°C.

A second set of models was run to test if the thermochronologic ages are compatible with either a reheating event during the Paleogene, the onset of volcanism in the late Eocene-early Oligocene, or early exhumation. The track-length distribution of sample KN85 (Fig. 4a) suggests that reheating could be possible. Geologically, reheating could be associated with volcanism prior to or during the early stages of rifting. To allow for this possibility, we reduced the temperature limits of the second boxes to 100°C and 10°C, thus permitting paths to reach lower temperatures at an earlier phase in the cooling history and extending the duration of this interval to between 40 and 20 Ma (Fig. 4c). Other constraints were similar to

the first run.

Well fitting HeFTy models for monotonic cooling of sample KN85 (Fig. 4a) suggest that a first episode of relatively rapid cooling (12°C/Myr) occurred from ~60 to 50 Ma. Subsequently, very slow cooling (~1.5°C/Myr) took place from ~45 Ma to ~15 Ma, followed by cooling to the present. As the model results are not well constrained over this final timeframe, we refrain from interpreting this cooling trend further. Because the model results rely on the calculating paths through the lowest temperature part of the PAZ and below the PAZ, where not much control on the thermal history exists, it is not known if cooling may have accelerated or not.

Using QTQt, we obtained results for the entire profile (Fig. 4b) that are broadly similar to the HeFTy results obtained for sample KN85 (Fig. 4a). Rapid cooling from about 65 to 50 Ma (~10°C/Myr) is followed by slow reheating (< 1°C/Myr) from ~40 to ~20 Ma. The model reveals a slight acceleration of cooling (~3°C/Myr) at ~15 Ma as part of a final continuous cooling episode, which has lasted to the present. Acceptable fits also permit an isothermal path without reheating from as early as ~50 Ma to as late as ~20 Ma. Despite some potential reheating of the uppermost samples within the transect between 40 and 20 Ma, the thermal histories for the different samples in the SH appear to have experienced similar t-T paths and are consistent with previous studies in the region (e.g., *Foster and Gleadow*, 1992; 1996). Acceptable fits for the reheating model using HeFTy (Fig. 4c) follow a broader swath than for the monotonic cooling model (Fig. 4a). The best fitting path shows that reheating is plausible. This scenario (Fig. 4c) shows rapid cooling (~10°C/Ma) from 55 to 40 Ma. Cooling was followed by a ~20 Ma interval at a near-constant temperature. A short-lived early Miocene pulse of reheating to temperatures as high as 100°C could have occurred, although a broad range of other paths that do not include reheating lie within the acceptable-fit envelope. Final cooling occurred from ~15 Ma to the present.

The QTQt reheating model results for the entire profile in the reheating scenario (Fig. 4d) show similar changes in the cooling rates. A first rapid cooling from ~65 to 50 Ma, reheating from ~50 to 35 Ma of ~2°C/Myr (particularly for the uppermost samples in the profile), then slow cooling from 35 to ~15Ma, and final cooling from ~15 Ma until the present (Fig. 4d). These results are quite similar to the previous QTQt modeling scenario (Fig. 4b).

From these two sets of models (monotonic cooling and reheating) and the general geologic context of the region, we conclude that reheating is permissible, but not required by the thermochronologic data. The differences between the two models suggest that the magnitude and timing of such a reheating event can only be loosely constrained (Figs. 4c and 4d).

4.4.2. Thermal modeling of data from the Northern Elgeyo Escarpment

Thermal models were run for the Northern Elgeyo Escarpment (NEE) profile in a similar manner as described above for the Samburu Hills profile. For the HeFTy (Fig. 5a) and QTQt (Fig. 5b) monotonic cooling models of sample KN102, the first constraint boxes were set to 160 to 10°C at 15 Ma to the present day. Second constraint boxes were set to ~150 to 30°C at 40 to 20 Ma for HeFTy and for QTQ, based on the AFT ages, sedimentary evidence in the hanging wall, and volcanic flows on top of the footwall. Third constraint boxes were set to 220 to 160°C at 75 to 40 Ma, based on an early to middle Tertiary regional extension with minor strain, which is also associated with the latest stages of extension of the Anza Rift in the north [*Foster and Gleadow*, 1996]. Again, HeFTy models always end with a constraint at the present-day surface temperature, ranging from 25 to 15°C, and QTQt models terminate at present-day temperatures ranging from 0° to 50°C

The second reheating model used similar constraints as the monotonic model, but

with slight changes in the time-temperature limits of the boxes. The second constraint box shows the most pronounced change, extending the range of temperatures from 120 to 10°C over a time range from 49 to 20 Ma in the HeFTy and QTQt models (Figs. 5b and 5d). This additional constraint permits reheating (by allowing for cooling to lower temperatures at an earlier period), which could be due to basaltic volcanism in the region starting in the northwest sector of Lake Turkana at ~37 Ma [i.e., *Zanettin et al., 1983; McDougall and Brown*, 2009] and farther south during the early Miocene (Samburu Basalts, ~20-11 Ma) [*Hackmann et al*. 1990] (Supplementary Figure 1).

HeFTy results for the monotonic cooling model for sample KN102 (Fig. 5a) display similar cooling paths as modeled for sample KN85 in the Samburu Hills (Fig. 4a). Rapid cooling (>20°C/Ma) from ~55 to 50 Ma is followed by very slow cooling (1.5°C/Myr) from 45 to 10 Ma, and finally moderate cooling of > 2.0°C/My until the present (Fig. 5a).

QTQt results from the entire profile at the Elgeyo Escarpment are broadly consistent with the HeFTy results, also showing rapid (>20°C/Myr) cooling from ~60 to 55 Ma. But rather than very slow cooling from ~50 to 15 Ma, the results show reheating (Fig. 5b). This reheating is followed by final cooling (~3°C/Ma) from 15 Ma to the present.

The HeFTy thermal model involving reheating (Fig. 5c) shows many similarities to the HeFTy model of monotonic cooling (Fig. 5a). The best fit of the reheating model exhibits relatively fast cooling rates (~15°C/Ma) from ~60 to 50 Ma and moderately fast cooling from ~50 to 30 Ma. Slight reheating follows from ~30 to 10 Ma; this reheating is followed by rapid cooling to the surface until the present. As observed for sample KN85 from the Samburu Hills (Figs. 4a, 4c), the broad envelope of the acceptable cooling paths shows that this model is not as tightly constrained as the monotonic cooling scenario (Fig. 5a). The second QTQt model has constraint boxes that were set between 160 to 10°C at 15 to 0 Ma, 120 to 10°C at 40 to 20 Ma, and 220 to 160°C at 75 to 45 Ma. The results show reheating constrained to a

shorter time window between ~35 and 10 Ma, even if the result looks forced by the constraint (Fig. 5d). For the remaining time windows, the QTQt modeling results agree with those from HeFTy.

4.4.3. Unconstrained thermal modeling of elevation profiles

In addition, we ran QTQt models for both regions without using any constraint boxes (Figs. 4e and 5e) to explore best fitting thermal histories when the program is set to freely search for acceptable solutions. The results do not differ substantially from the results of the constrained model runs described above. These results overall show that between periods of rapid cooling, the Samburu Hills profile may have experienced limited reheating, while the Northern Elgeyo Escarpment is likely to have experienced reheating. Ultimately, the modeling results are consistent, independent of the choice of the constraint boxes. Therefore, the input data, i.e. the ages and track lengths, guide the basic shape of the paths, rather than the user-defined constraint boxes. Other modeling results, including scenarios with short pulses of reheating, are provided in the supplementary material (Supplementary Figure 3)

Overall, results of the modeling with single (HeFTy) and multiple (QTQt) samples suggest a similar thermal history for the eastern and the western flanks of the northern and central Kenya Rift sectors, with clear periods of rapid cooling between ~65 and 50 Ma and from ~15 Ma to today, with either stable temperatures or reheating in between (Figs. 4 and 5).

5. Discussion

Our new thermochronological data and thermal modeling results from the Samburu Hills and the Elgeyo Escarpment of Kenya define three Cenozoic stages of thermal evolution: (1) rapid cooling between ~65 and ~50 Ma, (2) subsequent slow cooling or slight reheating

during the Oligo-Miocene, and (3) renewed rapid cooling after 15 Ma. Below, we address these different cooling stages with respect to rift evolution in Kenya and within the broader context of regional extensional processes in East Africa.

5.1. Paleocene to Eocene (65 – 50 Ma) rapid cooling

Our HeFTy and QTQt thermal modeling of samples from the Samburu Hills elevation profile on the eastern side of the rift valley and from the Elgeyo Escarpment on the western side yielded similar results, documenting rapid, early Cenozoic regional cooling (> 50°C) between ~65 and 50 Ma (Figs. 4 and 5). These results are in good agreement with previous modeling of apatite fission track and length parameters from samples collected in the Cherangani Hills and the basement rocks SE of Lake Turkana, which revealed 60 to 70°C of cooling between approximately 60 and 50 Ma [*Foster and Gleadow*, 1996; *Spiegel et al*., 2007]. This cooling appears to have been coeval with renewed extension and tectonic subsidence in the Anza Rift [i.e., *Morley et al., 1999b; Bosworth and Morley*, 1994; *Morley*, 2002], which is inferred to have been associated with flexural upwarping of rift flanks in that region [*Foster and Gleadow*, 1996].

5.2. Eocene through middle Miocene monotonic slow cooling or reheating

Our results show that very slow cooling or reheating occurred between ~45 and 15 Ma in the Samburu Hills and at the Northern Elgeyo Escarpment, with temperatures ranging between ~60° and 90°C from the Eocene through the middle Miocene. Similar results were reported by *Foster and Gleadow* [1996] and *Spiegel et al.* [2007], with very slow cooling along both the western (Cherangani Hills) and eastern (Ndoto Mountains) rift shoulders from the Eocene through the middle Miocene.

The models show that minor reheating is likely to have occurred from Eocene to

middle Miocene time (~45 to 15 Ma) for the Northern Elgeyo Escarpment samples, and is permitted, but not required for the Samburu Hills samples over a similar time interval. The Miocene phonolites are too young to explain this reheating. However, for the Northern Elgeyo Escarpment, reheating is compatible with geological interpretations of the early Cenozoic rifting phase in the Kerio Basin (Fig. 1a) based on seismic reflection data [*Mugisha et al.*, 1997; *Hautot et al.*, 2000]. The seismic reflection data document an early (as of yet undated) stage of tectonically controlled basin subsidence beneath the Neogene Kerio Basin followed by regional thermal basin subsidence and sedimentation within a sag basin [*Morley et al.*, 1992; *Mugisha et al.*, 1997; *Morley*, 1999a; *Hautot et al.*, 2000]. Thermo-chronological and geophysical evidence for protracted subsidence in this sag basin is corroborated by regional pinch-outs of fluvial and organic-rich lacustrine sediments exposed along the Elgeyo Escarpment [*Morley et al*, 1992; *Mugisha, 1997*; *Ego*, 1994; *Renaut et al.*, 1999] and the regional extent and thickness of the overlying <14.5 Ma phonolites that cover the present-day eastern and western rift shoulders [*Lippard, 1973*]. Alternatively, reheating could have been associated with the thermal impact of a mantle plume beneath the Tanzanian Craton since the Eocene-Oligocene [*Ebinger and Sleep*, 1998; *George et al.*, 1998; *Pik et al.*, 2008].

In this context, it is interesting that our thermochronologic data obtained from the Samburu Hills on the eastern rift shoulder exhibit a similar cooling history as samples from the Cherangani Hills on the western rift shoulder [*Foster and Gleadow*, 1996*; Spiegel et al.*, 2007] (Fig. 6), with reheating permitted, but not required. Due to their locations on the rift shoulders, neither area was affected by reheating related to subsidence and sedimentation within a sag basin. Thermal impacts of a mantle plume beneath the Tanzanian Craton since the Eocene-Oligocene [*Ebinger and Sleep*, 1998; *George et al.*, 1998; *Pik et al.*, 2008] remain a possibility, but clearly did not strongly influence the thermal evolution of the area as recorded in our samples.

5.3. Middle Miocene – Recent renewed cooling

Our thermal modeling shows a renewed, rapid cooling event starting at ~15 Ma in the Samburu Hills and the northern Elgeyo Escarpment, with rocks cooling from temperatures of ~60°C in the Samburu Hills and from ~90°C at the northern Elgeyo Escarpment. This accelerated cooling is compatible with the tectono-magmatic and sedimentary evolution of the northern and central Kenya rifts. Extensional faulting and the generation of transfer faults guided by foliation and inherited brittle shear zones in the Proterozoic basement gneisses affected the <14.5-m.y.-old phonolites as well as undated lacustrine shales, arkosic sandstones, and conglomerates [*Hetzel and Strecker*, 1994; *Ogola et al.*, 1994; *Ego*, 1994], now exposed on the rift shoulders at the Elgeyo escarpment (Fig. 6). These processes were responsible for the formation of a second rift basin superposed on the Paleogene basin (Fig. 6). This younger basin has the geometry of a down-to-the-east halfgraben, which hosts the present-day Kerio Basin. The Neogene phase of extension generated an additional 2 km of sedimentary and volcanic fill in addition to the 4 km of basin deposits that had been deposited during Paleogene rifting, with the corresponding bounding fault being located farther west [*Mugisha et al.*, 1997; *Morley, 1999; Hautot et al.*, 2000], (Fig. 6).

5.4. Regional implications for rifting in East Africa

Our thermochronological results from the Elgeyo and Samburu sites in the northern and central Kenya Rift sectors agree with the well-documented, regionally widespread Paleogene episode of extension in the Turkana region [*Morley et al.*, 1992; *Foster and Gleadow*, 1996; *Morley et al.*, 1999*; Morley*, 2002; *Tiercelin et al.*, 2012]. East of the present-day Elgeyo Escarpment, Paleogene normal faulting and coeval sedimentation along the proto-Kerio Basin had been previously inferred based on a pronounced negative Bouguer

gravity anomaly, reflecting a thick sedimentary fill, thought to be incompatible with the amount of Neogene extension and tectonic basin subsidence [*Morley et al.*, 1992; *Mugisha et al.*, 1997]. As neither currently available geophysical, geological, nor thermo-chronological data suggest similar coeval Paleogene extension processes in the central and southern sectors of the Kenya Rift, it appears that early Cenozoic rifting in Kenya was focused in the greater Turkana region [i.e., *Morley et al.*, 1992; *Foster and Gleadow*, 1992; *Foster and Gleadow*, 1996; *Morley*, 1999*; Spiegel et al.*, 2007], the Anza Rift, where Mesozoic extensional faults were reactivated [i.e., *Morley et al.*, 1999b*; Bosworth and Morley*, 1994], and regions as far south as the transition between the central and northern Kenya rifts (this study).

Thermo-chronologic data from other sectors of the EARS reveal spatially disparate and diachronous cooling histories (Fig. 7). Approximately 300 km to the southeast of the Elgeyo region, the Pangani Rift of northern Tanzania is the closest manifestation of Paleocene-Eocene extensional processes in the southern continuation of the eastern branch of the EARS. Apatite fission-track data indicate that a phase of rapid cooling began during the late Cretaceous and continued throughout the Paleogene [*Noble et al.*, 1997*; Mbede*, 2001], although no thermal modeling was performed to better constrain the timing. In the western branch of the EARS, the Rwenzori Mountains and the Albertine Rift of Uganda have a distinctly different late Cretaceous to Cenozoic thermal history, with very slow cooling of < 0.5°C/Myr from the late Cretaceous through the middle Eocene (70 to 40 Ma), and faster cooling (~1 to 4°C/Myr) from the middle Eocene at least through the Oligocene [*Bauer et al.*, 2013]. The Malawi Rift in Tanzania (western branch of the EARS) records a broadly similar history as the Rwenzoris Mountains over that time interval, with slow cooling from the Cretaceous through the Paleocene, and more rapid cooling (~0.5 to 1°C/Myr) starting after ~40 Ma [*van der Beek et al.*, 1998].

Sedimentologic, geomorphic, and geochronologic studies from different sectors of the

EARS also suggest diachronous, yet partly overlapping rift-related exhumation in East Africa (Fig. 7). For example, the Lake Rukwa region of the western branch and the rift basins west of Lake Turkana record an Oligocene onset of rifting [*Morley et al.*, 1992, 1999; *Roberts et al.*, 2012]. Our new data from the Elgeyo Escarpment combined with field observations by *Chapman et al.* [1978] and geophysical data from the Kerio Basin [*Mugisha et al.* 1997] also suggests an earlier onset of extensional processes in this región, while the present-day morphologic characteristics of northern and central Kenya rifts are the result of renewed normal faulting after 12 Ma, coeval with extension recorded in the Central Tanganyika Basin [*Chapman et al.*, 1978; *Baker et al.*, 1988; *Strecker et al.*, 1990], and the Albertine and southern Kenya rifts record the formation of extensional basin fills after approximately 9 and 7 Ma, respectively [*Crossley*, 1979; *Pickford and Senut*, 1994; *Lezzar et al.*, 1996].

At first sight, the regional data regarding extension the EARS summarized in Fig. 7 suggest an earlier onset of extension based on thermochronological data compared to stratigraphic information. This is probably an artifact, because sediments and volcanic rocks associated with Paleogene rifting have subsided, and coeval removal of rift-related deposits from exposed fault blocks and rift-shoulder areas precludes inspection of the early sedimentological vestiges of rifting. This problem is well emphasized by the Paleogene onset of rifting in the Kenyan Kerio Valley, where eroded sedimentary deposits from rift-shoulder areas have only been imaged by geophysical techniques [*Mugisha et al.*, 1997].

In any case, the available thermochronologic and geologic data reveals a spatially disparate and diachronous evolution of Cenozoic rifting in East Africa, with clear differences in the onset of rifting in the western and eastern branches of the EARS. This spatiotemporal pattern of extension is inconsistent with tectonic models of rifting in East Africa that are based on a southward-directed migration of volcanism and cogenetic extension [*McConnell*, 1972*; Ebinger and Sleep*, 1998; *Ebinger et al*. 2000; *Nyblade and Brazier*, 2002; *Morley,*

2010]. In light of the pronounced geophysical anomalies, evidence for mantle advection, and the evolution of dynamic topography associated with regional domal uplift [i.e., *White and McKenzie*, 1989; *Simiyu and Keller*, 1997; *Prodehl et al.*, 1997; *Achauer and Masson*, 2002*; Mechie et al., 1997*; *Sepulchre et al*., 2006; *Moucha and Forte*, 2011; *Wichura et al.*, 2015], the timing of extension throughout East Africa likely reflects a large-scale, mantle-driven process that generated differential stresses [e.g., *Crough*, 1983; *Zeyen et al.*, 1997] and the formation of rift basins in areas characterized by pronounced lithospheric and crustal-scale anisotropies and weaknesses [i.e., *Ashwal and Burke*, 1989; *Ebinger and Sleep*, 1998; *Smith and Mosley*, 1993; *Smith*, 1994]. As such, our new data from the Kenya Rift, combined with the synopsis of geological and thermo-chronological studies in East Africa, is compatible with recent numerical modeling results [*Koptev et al.*, 2015] that predict a regionally overlapping initiation of amagmatic and magmatic rifting sectors in East Africa following the asymmetric impingement of a single mantle plume [i.e., *Halldórsson et al.*, 2014] at the base of the lithosphere of the eastern sector of the Tanzania Craton.

6. Conclusions

Our new AFT and ZHe data from both escarpment and rift shoulders from the northern and central sectors of the Kenya Rift help to define two distinct stages of rapid cooling from ~65 to 45 Ma and from ~15 Ma to the present day, separated by a long phase of near-isothermal conditions or minor reheating. The initial stage of rapid cooling likely reflects the initiation of Cenozoic rifting, followed by a period of relative quiescence, and then renewed rift activity since the middle Miocene. While our thermal modeling results are consistent with those reported from the northern Kenya Rift and the Pangani Rift (e.g., the eastern branch of the EARS), they contrast markedly with those reported from the western branch (Rwenzori Mountains, and the Rukwa and Malawi rifts). As such, we suggest that the

spatiotemporal evolution of rifting in the EARS is compatible with the impact of mantle upwelling, ensuing crustal uplift, and extensional fracture propagation guided by crustal heterogeneities, rather than being related to the southward progression of mantle-plume activity.

Acknowledgments

V.T.A was supported by the DFG Graduate School GRK1364 *Shaping Earth´s Surface in a Variable Environment*, funded by the Deutsche Forschungsgemeinschaft (DFG) through a grant to M.R.S. (grant STR 373-20/1). We thank the Government of Kenya and the University of Nairobi for research permits and logistical support. T.F.S. was supported by the DFG's Emmy-Noether-Programme (grant number SCHI 1241/1-1). We thank Matthias Bernet, Lydia Olaka, Henry Wichura and Rod Brown for discussions. The data for this paper are available by contacting the corresponding author.

References

Achauer, U., and F. Masson (2002), Seismic tomography of continental rifts revisited: from relative to absolute heterogeneities, *Tectonophysics*, *358*(1–4), 17-37, doi:10.1016/S0040-1951(02)00415-8

Aljabri, S. S. (1992), Geology, mineralogy and geochemistry of fluorite mineralization in the Kerio Valley and Tugen Escarpment of Kenya. MSc thesis, 313 pp, University of Nairobi, Nairobi, Kenya.

Ashwal, L. D., and K. Burke (1989), African lithospheric structure, volcanism, and topography, *Earth and Planetary Science Letters*, *96*(1–2), 8-14, doi:10.1016/0012-821x(89)90119-2

Bailey, G. N., and G. C. P. King (2011), Dynamic landscapes and human dispersal patterns: tectonics, coastlines, and the reconstruction of human habitats, *Quaternary Science Reviews*, *30*(11–12), 1533-1553, doi:10.1016/j.quascirev.2010.06.019

Baker, B. H., J. G. Mitchell, and L. A. J. Williams (1988), Stratigraphy, geochronology and volcano-tectonic evolution of the Kedong–Naivasha–Kinangop region, Gregory Rift Valley, Kenya, *Journal of the Geological Society*, *145*(1), 107-116, doi:10.1144/gsjgs.145.1.0107

Bauer, F. U., U. A. Glasmacher, U. Ring, A. Schumann, and B. Nagudi (2010), Thermal and exhumation history of the central Rwenzori Mountains, Western Rift of the East African

Rift System, Uganda, *International Journal of Earth Sciences*, *99*(7), 1575-1597, doi:10.1007/s00531-010-0549-7

Bauer, F. U., M. Karl, U. A. Glasmacher, B. Nagudi, A. Schumann, and L. Mroszewski (2012), The Rwenzori Mountains of western Uganda - Aspects on the evolution of their remarkable morphology within the Albertine Rift, *Journal of African Earth Sciences*, *73-74*, 44-56, doi:10.1016/j.jafrearsci.2012.07.001

Bauer, F. U., U. A. Glasmacher, U. Ring, M. Karl, A. Schumann, and B. Nagudi (2013), Tracing the exhumation history of the Rwenzori Mountains, Albertine Rift, Uganda, using low-temperature thermochronology, *Tectonophysics*, *599*(C), 8-28, doi:10.1016/j.tecto.2013.03.032

Bobe, R., and A. K. Behrensmeyer (2004), The expansion of grassland ecosystems in Africa in relation to mammalian evolution and the origin of the genus Homo, *Palaeogeography, Palaeoclimatology, Palaeoecology*, *207*(3–4), 399-420, doi:10.1016/j.palaeo.2003.09.033

Bosworth, W., and A. Maurin (1993), Structure, geochronology and tectonic significance of the northern Suguta Valley (Gregory Rift), Kenya, *Journal of the Geological Society*, *150*(4), 751-762, doi:10.1144/gsjgs.150.4.0751

Bosworth, W., and C. K. Morley (1994), Structural and stratigraphic evolution of the Anza rift, Kenya, *Tectonophysics*, *236*(1–4), 93-115, doi:10.1016/0040-1951(94)90171-6

Burke, K. (1996), The African plate, *South African Journal of Geology*, *99*(4), 341-409.

Chapman, G. R., S. J. Lippard, and J. E. Martyn (1978), The stratigraphy and structure of the Kamasia Range, Kenya Rift Valley, *Journal of the Geological Society*, *135*(3), 265-281, doi:10.1144/gsjgs.135.3.0265

Cohen, A. S., M. J. Soreghan, and C. A. Scholz (1993), Estimating the age of formation of lakes: An example from Lake Tanganyika, East African Rift system, *Geology*, *21*(6), 511-514, doi:10.1130/0091-7613(1993)021<0511:etaofo>2.3.co;2

Crossley, R. (1979), The Cenozoic stratigraphy and structure of the western part of the Rift Valley in southern Kenya, *Journal of the Geological Society*, *136*(4), 393-405, doi:10.1144/gsjgs.136.4.0393

Crough, T. S. (1983), Rifts and swells: Geophysical constraints on causality, *Tectonophysics*, *94*(1–4), 23-37, doi:10.1016/0040-1951(83)90007-0

Dobson, K. J. (2006), The zircon (U-Th)/He thermochronometer: development and application of thermochronometers in igneous provinces, Ph.D Thesis, University of Glasgow, Glasgow, Scotland, 241.

Dobson, K. J., C. Persano, and F. M. Stuart (2009), Quantitative constraints on mid- to shallow-crustal processes using the zircon (U–Th)/He thermochronometer, *Geological Society, London, Special Publications*, *324*(1), 47-56, doi:10.1144/sp324.4

Donelick, R. A., R. A. Ketcham, and W. D. Carlson (1999), Variability of apatite fission-track annealing kinetics: II. Crystallographic orientation effects, *Am. Mineral.*, *84*(9), 1224-1234.

Donelick, R. A., P. B. O'Sullivan, and R. A. Ketcham (2005), Apatite Fission-Track Analysis, *Reviews in Mineralogy and Geochemistry*, *58*(1), 49-94, doi:10.2138/rmg.2005.58.3

Ebinger, C. J., and N. H. Sleep (1998), Cenozoic magmatism throughout east Africa resulting from impact of a single plume, *Nature*, *395*(6704), 788-791, doi:10.1038/27417

Ebinger, C. J., T. Yemane, D. J. Harding, S. Tesfaye, S. Kelley, and D. C. Rex (2000), Rift

deflection, migration, and propagation: Linkage of the Ethiopian and Eastern rifts, Africa, Geological Society of America Bulletin, 112(2), 163-176, doi:10.1130/0016-7606(2000)112<163:rdmapl>2.0.co;2

Ebinger, C., and C. A. Scholz (2012), Continental Rift Basins: The East African Perspective, in *Tectonics of Sedimentary Basins*, pp. 183-208, John Wiley & Sons, Ltd, doi:10.1002/9781444347166.ch9

Ego, J. K. (1994), Sedimentology and diagenesis of Neogene sediments in the Central Kenya Rift Valley, MSc thesis, University of Saskatchewan, Saskatoon, 1-148.

Ehlers, T. A., and K. A. Farley (2003), Apatite (U-Th)/He thermochronometry: methods and applications to problems in tectonic and surface processes, *Earth and Planetary Science Letters*, *206*(1–2), 1-14, doi:10.1016/s0012-821x(02)01069-5

Farley, K. A., and D. F. Stockli (2002), (U-Th)/He Dating of Phosphates: apatite, monazite, and xenotime, *Reviews in Mineralogy and Geochemistry*, *48*(1), 559-577, doi:10.2138/rmg.2002.48.15

Farley, K. A., R. A. Wolf, and L. T. Silver (1996), The effects of long alpha-stopping distances on (U-Th)/He ages, *Geochimica et Cosmochimica Acta*, *60*(21), 4223-4229, doi:10.1016/s0016-7037(96)00193-7

Fitzgerald, P. G. (1992), The Transantarctic Mountains of southern Victoria Land: The application of apatite fission track analysis to a rift shoulder uplift, *Tectonics*, *11*, 634-662, doi:10.1029/91tc02495

Flannery, J. W., and B. R. Rosendahl (1990), The seismic stratigraphy of Lake Malawi, Africa: implications for interpreting geological processes in lacustrine rifts, *Journal of African Earth Sciences*, *10*(3), 519-548, doi:10.1016/0899-5362(90)90104-m

Flowers, R. M. (2009), Exploiting radiation damage control on apatite (U–Th)/He dates in cratonic regions, *Earth and Planetary Science Letters*, *277*(1–2), 148-155, doi:10.1016/j.epsl.2008.10.005

Flowers, R. M., D. L. Shuster, B. P. Wernicke, and K. A. Farley (2007), Radiation damage control on apatite (U-Th)/He dates from the Grand Canyon region, Colorado Plateau, *Geology*, *35*(5), 447-450, doi:10.1130/g23471a.1

Foeken, J. P. T., F. M. Stuart, K. J. Dobson, C. Persano, and D. Vilbert (2006), A diode laser system for heating minerals for (U-Th)/He chronometry, *Geochemistry, Geophysics, Geosystems*, *7*(4), Q04015, doi:10.1029/2005gc001190

Foster, A., C. Ebinger, E. MBede, and D. Rex (1997), Tectonic development of the northern Taiizaiiian sector of the East African Rift System, *Journal of the Geological Society*, *154*(4), 689-700, doi:10.1144/gsjgs.154.4.0689

Foster, D. A., and A. J. W. Gleadow (1992), The morphotectonic evolution of rift-margin mountains in central Kenya: Constraints from apatite fission-track thermochronology, *Earth and Planetary Science Letters*, *113*(1–2), 157-171, doi:10.1016/0012-821x(92)90217-j

Foster, D. A., and A. J. W. Gleadow (1996), Structural framework and denudation history of the flanks of the Kenya and Anza Rifts, East Africa, *Tectonics*, *15*(2), 258-271, doi:10.1029/95tc02744

Fox, M., and D. L. Shuster (2014), The influence of burial heating on the (U–Th)/He system in apatite: Grand Canyon case study, *Earth and Planetary Science Letters*, 397(C), 174-

183, doi:10.1016/j.epsl.2014.04.041

Frostick, L. E., and I. Reid (1990), Structural control of sedimentation patterns and implication for the economic potential of the East African Rift basins, *Journal of African Earth Sciences (and the Middle East)*, *10*(1–2), 307-318, doi:10.1016/0899-5362(90)90062-j

Galbraith, R. F. (1981), On statistical models for fission track counts, *Mathematical Geology*, *13*(6), 471-478, doi:10.1007/bf01034498

Gallagher, K., J. Stephenson, R. Brown, C. Holmes, and P. Ballester (2005), Exploiting 3D Spatial Sampling in Inverse Modeling of Thermochronological Data, *Reviews in Mineralogy and Geochemistry*, *58*(1), 375-387, doi:10.2138/rmg.2005.58.14

Gallagher, K. (2012), Transdimensional inverse thermal history modeling for quantitative thermochronology, *Journal of Geophysical Research: Solid Earth*, *117*(B2), B02408, doi:10.1029/2011jb008825

Gallagher, K., K. Charvin, S. Nielsen, M. Sambridge, and J. Stephenson (2009), Markov chain Monte Carlo (MCMC) sampling methods to determine optimal models, model resolution and model choice for Earth Science problems, *Marine and Petroleum Geology*, *26*(4), 525-535, doi:10.1016/j.marpetgeo.2009.01.003

Gautheron, C., L. Tassan-Got, J. Barbarand, and M. Pagel (2009), Effect of alpha-damage annealing on apatite (U-Th)/He thermochronology, *Chemical Geology*, *266*(3–4), 157-170, doi:10.1016/j.chemgeo.2009.06.001

George, R., N. Rogers, and S. Kelley (1998), Earliest magmatism in Ethiopia: Evidence for two mantle plumes in one flood basalt province, *Geology*, *26*(10), 923-926, doi:10.1130/0091-7613(1998)026<0923:emieef>2.3.co;2

Green, P. F., P. V. Crowhurst, I. R. Duddy, P. Japsen, and S. P. Holford (2006), Conflicting (U-Th)/He and fission track ages in apatite: Enhanced He retention, not anomalous annealing behaviour, *Earth and Planetary Science Letters*, *250*(3–4), 407-427, doi:10.1016/j.epsl.2006.08.022

Hackman, B., T. Charsley, R. Key, and A. Wilkinson (1990), The development of the East African Rift system in north-central Kenya, *Tectonophysics*, *184*(2), 189-211, doi:10.1016/0040-1951(90)90053-b

Halldórsson, S. A., D. R. Hilton, P. Scarsi, T. Abebe, and J. Hopp (2014), A common mantle plume source beneath the entire East African Rift System revealed by coupled helium-neon systematics, *Geophysical Research Letters*, *41*(7), 2304-2311, doi:10.1002/2014GL059424

Hansen, K., and P. W. Reiners (2006), Low temperature thermochronology of the southern East Greenland continental margin: Evidence from apatite (U–Th)/He and fission track analysis and implications for intermethod calibration, *Lithos*, *92*(1–2), 117-136, doi:10.1016/j.lithos.2006.03.039

Hautot, S., P. Tarits, K. Whaler, B. Le Gall, J.-J. Tiercelin, and C. Le Turdu (2000), Deep structure of the Baringo Rift Basin (central Kenya) from three-dimensional magnetotelluric imaging: Implications for rift evolution, *Journal of Geophysical Research: Solid Earth*, *105*(B10), 23493-23518, doi:10.1029/2000jb900213

Hetzel, R., and M. R. Strecker (1994), Late Mozambique Belt structures in western Kenya and their influence on the evolution of the Cenozoic Kenya Rift, *Journal of Structural*

Geology, *16*(2), 189-201, doi:10.1016/0191-8141(94)90104-x

Hurford, A. J., and P. F. Green (1983), The zeta age calibration of fission-track dating, *Chemical Geology*, *41*(0), 285-317, doi:10.1016/s0009-2541(83)80026-6

Ketcham, R. A., R. A. Donelick, and W. D. Carlson (1999), Variability of apatite fission-track annealing kinetics: III. Extrapolation to geological time scales, *American Mineralogist*, 84(9), 1235-1255.

Ketcham, R. A. (2005), Forward and Inverse Modeling of Low-Temperature Thermochronometry Data, *Reviews in Mineralogy and Geochemistry*, *58*(1), 275-314, doi:10.2138/rmg.2005.58.11

Ketcham, R. A., R. A. Donelick, M. L. Balestrieri, and M. Zattin (2009), Reproducibility of apatite fission-track length data and thermal history reconstruction, *Earth and Planetary Science Letters*, *284*(3–4), 504-515, doi:10.1016/j.epsl.2009.05.015

Koehn, D., K. Aanyu, S. Haines, and T. Sachau (2008), Rift nucleation, rift propagation and the creation of basement micro-plates within active rifts, *Tectonophysics*, *458*(1–4), 105-116, doi:10.1016/j.tecto.2007.10.003

Koptev, A., E. Calais, E. Burov, S. Leroy, and T. Gerya (2015), Dual continental rift systems generated by plume-lithosphere interaction, *Nature Geoscience*, *8*(5), 388-392, doi:10.1038/ngeo2401

Levin, N. E., E. J. Zipser, and T. E. Cerling (2009), Isotopic composition of waters from Ethiopia and Kenya: Insights into moisture sources for eastern Africa, *Journal of Geophysical Research: Atmospheres*, *114*(D23), D23306, doi:10.1029/2009jd012166

Lezzar, K. E., J. J. Tiercelin, M. D. Batist, A. S. Cohen, T. Bandora, P. V. Rensbergen, C. L. Turdu, W. Mifundu, and J. Klerkx (1996), New seismic stratigraphy and Late Tertiary history of the North Tanganyika Basin, East African Rift system, deduced from multichannel and high-resolution reflection seismic data and piston core evidence, *Basin Research*, *8*(1), 1-28, doi:10.1111/j.1365-2117.1996.tb00112.x

Lippard, S. J. (1973), The petrology of phonolites from the Kenya Rift, *Lithos*, *6*(3), 217-234, doi:10.1016/0024-4937(73)90083-2

Maboko, M. A. H., N. A. I. M. Boelrijk, H. N. A. Priem, and E. A. T. Verdurmen (1985), Zircon U-Pb and biotite Rb-Sr dating of the wami river granulites, Eastern Granulites, Tanzania: Evidence for approximately 715 Ma old granulite-facies metamorphism and final Pan-African cooling approximately 475 Ma ago, *Precambrian Research*, *30*(4), 361-378, doi:10.1016/0301-9268(85)90088-9

MBede, E. (2001), Tectonic setting and uplift analyiss of the Pangani Rift Basin in Northern Tanzania Using Apatite fission Track Thermochronology, in *Tanzanian Journal of Sciences*, *27*(2) 1-16, doi:10.4314/tjs.v27i2.18344

McConnell, R. (1972), Geological development of the rift system of East Africa, *Geological Society of America Bulletin*, *83*(9), 2549-2572, doi:10.1144/gsl.sp.1978.006.01.04

McDougall, I., and F. H. Brown (2009), Timing of volcanism and evolution of the northern Kenya Rift, *Geol. Mag.*, *146* (1), 34-47, doi:10.1017/s0016756808005347

Mechie, J., C. Prodehl, K. G.R, M. A. Khan, and S. J. Gaciri (1997), A model for structure, composition and evolution of the Kenya rift, *Tectonophysics*, *278*(1-4) 95-119, doi:10.1016/s0040-1951(97)00097-8

Melnick, D., Y. Garcin, J. Quinteros, M. R. Strecker, D. Olago, and J. J. Tiercelin (2012), Steady rifting in northern Kenya inferred from deformed Holocene lake shorelines of the Suguta and Turkana basins, *Earth and Planetary Science Letters*, *331*, 335-346, doi:10.1016/j.epsl.2012.03.007

Michon, L. (2015), What the volcanism of the East African Rift tells us on its evolution and dynamics: a reappraisal, *Geophysical Research Abstracts*, *17*, EGU2015-3407.

Morley, C. K., W. A. Wescott, D. M. Stone, R. M. Harper, and F. M. Karanja (1992), Tectonic evolution of the northern Kenya Rift, *Journal of the Geological Society, 149*, 333-348, doi:0.1144/gsjgs.149.3.0333

Morley, C., and D. Ngenoh (1999), Introduction to the East African Rift System, in *Studies in Geology # 44, AAPG*, 1-18.

Morley, C., W. Bosworth, R. Day, R. Lauck, R. Bosher, D. Stone, S. Wigger, W. Wescott, D. Haun, and N. Bassett (1999b), Geology and Geophysics of the Anza Graben, in *Studies in Geology # 44, AAPG*, 67-90.

Morley, C. K. (2002), Tectonic Settings of Continental Extensional Provinces and Their Impact on Sedimentation and Hydrocarbon Prospectivity, in *Sedimentation in Continental Rifts*, edited by R. W. Renaut and G. M. Ashley, p. 329, *Society for Sedimentary Geology (SEPM)*, doi:10.2110/pec.02.73.0025

Morley, C. K. (2010), Stress re-orientation along zones of weak fabrics in rifts: An explanation for pure extension in 'oblique' rift segments?, *Earth and Planetary Science Letters*, *297*(3–4), 667-673, doi:10.1016/j.epsl.2010.07.022

Moucha, R., and A. M. Forte (2011), Changes in African topography driven by mantle convection, *Nature Geoscience*, *4*(10), 707-712, doi:10.1038/ngeo1235

Mugisha, F., C. J. Ebinger, M. Strecker, and D. Pope (1997), Two-stage rifting in the Kenya rift: implications for half-graben models, *Tectonophysics*, *278*(1-4), 63-81, doi: 10.1016/s0040-1951(97)00095-4

Noble, W. P., D. A. Foster, and A. J. W. Gleadow (1997), The post-Pan-African thermal and extensional history of crystalline basement rocks in eastern Tanzania, *Tectonophysics*, *275*(4), 331-350, doi:10.1016/s0040-1951(97)00026-7

Nyblade, A. A., T. J. Owens, H. Gurrola, J. Ritsema, and C. A. Langston (2000), Seismic evidence for a deep upper mantle thermal anomaly beneath east Africa, *Geology*, *28*(7), 599-602, doi:10.1130/0091-7613(2000)28<599:sefadu>2.0.co;2

Nyblade, A., and R. Brazier (2002), Precambrian lithospheric controls on the development of the East African rift system, *Geology*, *30*(8), 755, doi:10.1130/0091-7613(2002)030<0755:plcotd>2.0.co;2

Odada, E. O., and D. O. Olago (2002), The East African Great Lakes: Limnology,Paleolimnology and Biodiversity, Kluwer Academic Publishers, The Netherlands, doi: 10.1007/0-306-48201-0

Ogola, J. S., H. J. Behr, and A. M. van den Kerkhof (1994), Fluid inclusion and cathodoluminescence studies on fluorite from the Kerio valley, Kenya, *Journal of African Earth Sciences*, *18*(4), 309-323, doi:10.1016/0899-5362(94)90070-1

Persano, C., F. M. Stuart, P. Bishop, and D. N. Barfod (2002), Apatite (U–Th)/He age constraints on the development of the Great Escarpment on the southeastern Australian passive margin, *Earth and Planetary Science Letters*, *200*(1–2), 79-90, doi:

10.1016/s0012-821x(02)00614-3

Pickford, M., & Senut, B., (1994) Palaeobiology of the Albertine Rift Valley: General conclusions and synthesis, in Geology and palaeobiology of the Albertine Rift Valley, Uganda-Zaire edited by Senut, B., & Pickford, pp. 409-423, *CIFEG Occasional Publication*, Orléans.

Pik, R., B. Marty, J. Carignan, G. Yirgu, and T. Ayalew (2008), Timing of East African Rift development in southern Ethiopia: Implication for mantle plume activity and evolution of topography, *Geology*, *36*(2), 167-170, doi:10.1130/g24233a.1

Prenzel, J., F. Lisker, M. L. Balestrieri, A. Läufer, and C. Spiegel (2013), The Eisenhower Range, Transantarctic Mountains: Evaluation of qualitative interpretation concepts of thermochronological data, *Chemical Geology*, *352*, 176-187, doi:10.1016/j.chemgeo.2013.06.005

Prodehl, C., D. Fuchs, and J. Mechie (1997), Seismic-refraction studies of the Afro-Arabian rift system -a brief review, *Tectonophysics*, *278*(1-4), 1-13, doi:10.1016/s0040-1951(97)00091-7

Reiners, P. W. (2005), Zircon (U-Th)/He thermochronometry, *Rev. Mineral Geochem.*, *58*, 151-179. Chantilly, Virginia, doi:10.2138/rmg.2005.58.6

Reiners, P. W., and M. T. Brandon (2006), Using thermochronology to understand orogenic erosion, *Annual Review of Earth and Planetary Sciences*, *34*, 419-466, doi:10.1146/annurev.earth.34.031405.125202

Renaut, R. W., J. K. Ego, J. J. Tiercelin, C. Le Turdu, and R. B. Owen (1999), Saline, alkaline palaeolakes of the Tugen Hills–Kerio Valley region, Kenya Rift Valley, in *Late Cenozoic environments and hominid evolution: A Tribute to Bill Bishop*, edited by P. Andrews and P. Banham, pp. 41-58 *The Geological Society of London*, London.

Richardson, C. K., and H. D. Holland (1979), Fluorite deposition in hydrothermal systems, *Geochimica et Cosmochimica Acta*, *43*(8), 1327-1335, doi:10.1016/0016-7037(79)90122-4

Roberts, E. M., N. J. Stevens, P. M. O'connor, P. H. G. M. Dirks, M. D. Gottfried, W. C. Clyde, R. A. Armstrong, A. I. S. Kemp, and S. Hemming (2012), Initiation of the western branch of the East African Rift coeval with the eastern branch, *Nature Geoscience*, *5*(4), 289-294, doi:10.1038/ngeo1432

Saneyoshi, M., K. Nakayama, T. Sakai, Y. Sawada, and H. Ishida (2006), Half graben filling processes in the early phase of continental rifting: The Miocene Namurungule Formation of the Kenya Rift, *Sedimentary Geology*, *186*(1), 111-131, doi:10.1016/j.sedgeo.2005.11.012

Scholz, C. A., and B. P. Finney (1994), Late Quaternary sequence stratigraphy of Lake Malawi (Nyasa), Africa, *Sedimentology*, *41*(1), 163-179, doi:10.1111/j.1365-3091.1994.tb01397.x

Schull, T. J. (1988), Rift basins of interior Sudan: Petroleum Exploration and Discovery, *AAPG Bulletin*, *72*(10), 1128-1142, doi:10.1306/703c9965-1707-11d7-8645000102c1865d

Sepulchre, P., G. Ramstein, F. d. r. Fluteau, M. Schuster, J.-J. Tiercelin, and M. Brunet (2006), Tectonic uplift and eastern Africa aridification, *Science*, *313*(5792), 1419-1423, doi:10.1126/science.1129158

Shackleton, R. M. (1993), Tectonics of the Mozambique Belt in East Africa, *The Geological*

Society of London, Special Publications, *76*(1), 345-362, doi:10.1144/gsl.sp.1993.076.01.17

Simiyu, S. M., and G. R. Keller (1997), An integrated analysis of lithospheric structure across the East African plateau based on gravity anomalies and recent seismic studies, *Tectonophysics*, *278*(1–4), 291-313, doi:10.1016/s0040-1951(97)00109-1

Smith, M. (1994), Stratigraphic and Structural Constraints on Mechanisms of Active Rifting in the Gregory Rift, Kenya, *Tectonophysics*, *236*(1-4), 3-22, doi:10.1016/0040-1951(94)90166-x

Smith, M., and P. Mosley (1993), Crustal heterogeneity and basement influence on the development of the Kenya Rift, East Africa, *Tectonics*, *12*(2), 591-606, doi:10.1029/92tc01710

Sobel, E. R., and D. Seward (2010), Influence of etching conditions on apatite fission-track etch pit diameter, *Chemical Geology*, *271*(1–2), 59-69, doi:10.1016/j.chemgeo.2009.12.012

Spiegel, C., B. P. Kohn, D. X. Belton, and A. J. W. Gleadow (2007), Morphotectonic evolution of the central Kenya rift flanks: Implications for late Cenozoic environmental change in East Africa, *Geology*, *35*(5), 427-430, doi:10.1130/g23108a.1

Strecker, M. R., P. M. Blisniuk, and G. H. Eisbacher (1990), Rotation of extension direction in the central Kenya Rift, *Geology*, *18*(4), 299-302, doi:10.1130/0091-7613(1990)018<0299:roedit>2.3.co;2

Tiercelin, J. J., and K. E. Lezzar (2002), A 300 million years history of rift lakes in Central and East Africa: an updated broad review, in *The East African Great Lakes: Limnology, Palaeolimnology and Biodiversity: Advances in Global Change Research*, edited by E. Odada and D. Olago, Springer, pp. 3-60, doi:10.1007/0-306-48201-0_1

Tiercelin, J. J., P. Thuo, J.-L. Potdevin, and T. Nalpas (2012), Hydrocarbon Prospectivity in Mesozoic and Early–Middle Cenozoic Rift Basins of Central and Northern Kenya, Eastern Africa, in *Tectonics and sedimentation: Implications for petroleum systems*, edited by D. Gao, *AAPG Memoir 100*, 79-207, doi:10.1306/13351553m1001742

Tiercelin, J. J., J. L. Potdevin, C. K. Morley, M. R. Talbot, H. Bellon, A. Rio, B. Le Gall, and W. Vétel (2004), Hydrocarbon potential of the Meso-Cenozoic Turkana Depression, northern Kenya. I. Reservoirs: depositional environments, diagenetic characteristics, and source rock–reservoir relationships, *Marine and Petroleum Geology*, *21*(1), 41-62, doi:10.1016/j.marpetgeo.2003.11.007

van der Beek, P., E. MBede, P. Andriessen, and D. Delvaux (1998), Denudation history of the Malawi and Rukwa Rift flanks (East African Rift System) from apatite fission track thermochronology, *Journal of African Earth Sciences*, *26*(3), 363-385, doi:10.1016/s0899-5362(98)00021-9

van der Beek, P. A., P. G. Valla, F. Herman, J. Braun, C. Persano, K. J. Dobson, and E. Labrin (2010), Inversion of thermochronological age–elevation profiles to extract independent estimates of denudation and relief history — II: Application to the French Western Alps, *Earth and Planetary Science Letters*, *296*(1–2), 9-22, doi:10.1016/j.epsl.2010.04.032

Wagner, M., R. Altherr, and P. Van Den Haute (1992), Apatite fission-track analysis of Kenyan basement rocks: constraints on the thermotectonic evolution of the Kenya dome.

A reconnaissance study, *Tectonophysics*, *204*(1–2), 93-110, doi:10.1016/0040-1951(92)90272-8

Wheildon, J., P. Morgan, K. H. Williamson, T. R. Evans, and C. A. Swanberg (1994), Heat flow in the Kenya rift zone, *Tectonophysics*, *236*(1–4), 131-149, doi:10.1016/0040-1951(94)90173-2

Wichura, H., R. Bousquet, R. Oberhänsli, M. R. Strecker, and M. H. Trauth (2010), Evidence for middle Miocene uplift of the East African Plateau, *Geology*, *38*(6), 543-546, doi:10.1130/g31022.1

Wichura, H., L. L. Jacobs, A. Lin, M. J. Polcyn, F. K. Manthi, D. A. Winkler, M. R. Strecker, and M. Clemens (2015), A 17-My-old whale constrains onset of uplift and climate change in east Africa, *Proceedings of the National Academy of Sciences*, *112*(13), 3910-3915, doi:10.1073/pnas.1421502112

White, R., and D. McKenzie (1989), Magmatism at Rift Zones: The generation of volcanic continental margins and flood basalts, *Journal of Geophysical Research*, *94*(B6), 7685-7729, doi:10.1029/jb094ib06p07685

Wolf, R. A., K. A. Farley, and D. M. Kass (1998), Modeling of the temperature sensitivity of the apatite (U-Th)/He thermochronometer, *Chemical Geology*, 148(1-2), 105-114, doi:10.1016/s0009-2541(98)00024-2

Zanettin, B., J. Visentin, E. Bellieni, E. M. Piccirillo, and F. Rita (1983), Le volcanisme du bassin du Nord-Turkana (Kenya): age, succession et evolution structurale, *Bull. Cent. Rech. Explor. Prod. Elf-Aquitaine, 7*, 249-255.

Zeyen, H., F. Volker, V. Wehrle, K. Fuchs, S. V. Sobolev, and R. Altherr (1997), Styles of continental rifting: crust-mantle detachment and mantle plumes, *Tectonophysics*, *278*, 329-352, doi:10.1016/s0040-1951(97)00111-x

Table 1. Apatite Fission Track (AFT) data from the Kenya Rift[a]

Sample	Latitude (°N)	Longitude (°E)	elev m asl	Lithology	Xl	Rho-S x10^6	NS	Rho-I x105	NI	P(χ^2) %	RhoD x10^6	ND	Age[b] Ma	±1σ Ma	Dpar mean	Dpar SD	n lengths	Mean length µm	SD µm	Analyst
Central Elgeyo Escarpment																				
KN50	35.5	0.6	1260	gneiss	20	1.497	279	2.873	1454	3	1.222	4978	43.2	3	2.3	0.2	0	-	-	AB
Southern Elgeyo Escarpment																				
KN53	35.6	0.3	1616	gneiss	20	2.173	68	0.566	2612	82	1.185	4978	5.7	1	2.3	0.2	5	13.2	3.6	AB
KN55	35.6	0.3	1440	gneiss	20	4.108	99	1.057	3849	100	1.136	4978	5.4	1	2.3	0.2	0	-	-	AB
KN90	35.6	0.4	1395	gneiss	18	1.583	32	0.393	1289	100	1.365	5713	6.3	1	1.9	0.2	0	-	-	AB
KN91	35.6	0.3	1776	gneiss	20	0.965	40	0.356	1086	100	1.359	5713	9.2	2	2.0	0.2	0	-	-	AB
KN92	35.6	0.3	1583	gneiss	23	1.880	44	0.346	2392	97	1.353	5713	4.6	1	1.9	0.2	0	-	-	AB
KN94	35.6	0.3	1389	gneiss	20	1.497	279	2.873	1454	100	1.347	5713	6	1	2.2	0.3	0	-	-	AB
Northern Elgeyo Escarpment																				
KN97[c]	35.6	0.7	1289	gneiss	20	1.340	95	1.326	960	66	1.438	5713	26.2	3	2.1	0.2	0	-	-	AB, VT
KN99	35.5	0.7	1480	gneiss	17	2.281	45	0.555	1850	89	1.426	5713	38	2	2.2	0.1	65	11.2	2.1	AB, VT
KN100	35.5	0.7	1559	gneiss	16	3.107	269	4.271	1957	99	1.420	5713	36	3	2.2	0.2	56	11.8	1.87	AB
KN102[c]	35.5	0.7	1852	gneiss	20	1.404	193	2.102	1289	10	1.407	5713	38.8	3	2.1	0.2	101	11.2	2.0	AB, VT
Samburu Hills																				
KN83	36.9	2.0	1487	gneiss	20	2.087	327	3.228	2114	30	1.401	5713	39.4	3	2.1	0.3	40	12.2	1.9	AB, VT
KN85[c]	36.9	2.0	1601	gneiss	20	1.836	195	1.836	1289	100	1.389	5713	38.7	3	2.2	0.2	100	11.9	1.9	AB, VT
KN89	36.9	2.0	1852	gneiss	11	0.574	56	1.144	281	100	1.371	5713	50.3	8	1.7	0.3	2	12.4	0.2	AB

[a] Sample preparation and analysis similar to that used by Sobel & Strecker (2003). All apatites were etched in 5.5 mol Nitric acid for 2o seconds at 21°. Samples analized with a Leica DMRM microscope with drawing tube located above a digitalizing tablet and a kinetek computer-controlled stage driven by the Ftstage program (Dimitru, 1993). Analysis was performed with reflected and transmited light at 1250x magnification. Samples were irradiated at Oregon State University. Following irradiation, the mica external detectors were etched with 21°C, 40%hydroflouric acid for 45 minutes. The pooled age is reported for samples with P(χ2) grater than (less than) 5% as they pass (fail) the χ2 test. Age errors are presented as one sigma, calculated using the zeta calibration method (Hurford and Green, 1983), AB:369.5±7.9, unpublished, 2012.

[b] Pooled age is reported for most of the samples, exept for sample KN50, central age is reported

[c] ^{252}Cf irradiations on additional grain mount of the sample

Table 2. (U-Th)/He ages of Zircon (ZHe) in The Kenya Rift.

Sample	Latitude (°N)	Longitude (°E)	elev m asl	U (ng)	Th (ng)	4He (cc)	Ft	Corrected age Ma	error (1σ) Ma	mineral
					Southern Elgeyo					
KN91	35.611	0.302	1776	6.7	91.9	6.87E-07	0.85	70.5	7.2	Zircon
KN91	35.611	0.302	1776	7.0	88.5	3.48E-07	0.85	37.3	3.8	Zircon
KN92	35.611	0.302	1583	14.0	34.2	1.07E-07	0.78	30.4	3.1	Zircon
KN92	35.611	0.302	1583	5.1	18.7	9.63E-08	0.74	54.0	5.5	Zircon
KN94	35.611	0.302	1389	9.5	41.7	1.74E-07	0.82	39.6	4.1	Zircon
KN94	35.611	0.302	1389	6.0	23.9	2.29E-07	0.82	89.8	9.2	Zircon
KN94	35.611	0.302	1389	9.1	42.3	1.74E-07	0.79	40.8	4.2	Zircon
					Northern Elgeyo					
KN97	35.552	0.660	1289	3.6	7.5	5.03E-08	0.83	59.7	6.1	Zircon
KN102	35.539	0.660	1852	15.9	28.6	1.83E-07	0.84	54.9	5.6	Zircon
KN102	35.539	0.660	1852	0.3	0.9	5.79E-09	0.82	58.9	6.1	Zircon
KN102	35.539	0.660	1852	8.6	18.5	1.64E-07	0.81	81.3	8.3	Zircon
KN102	35.539	0.660	1852	13.7	32.7	1.94E-07	0.82	54.1	5.5	Zircon
					Samburu Hills					
KN85	36.875	2.032	1600	1.7	1.5	9.06E-09	0.78	50.8	5.2	Zircon
KN85	36.875	2.032	1600	1.3	1.0	6.54E-09	0.81	50.5	5.2	Zircon

Figure captions

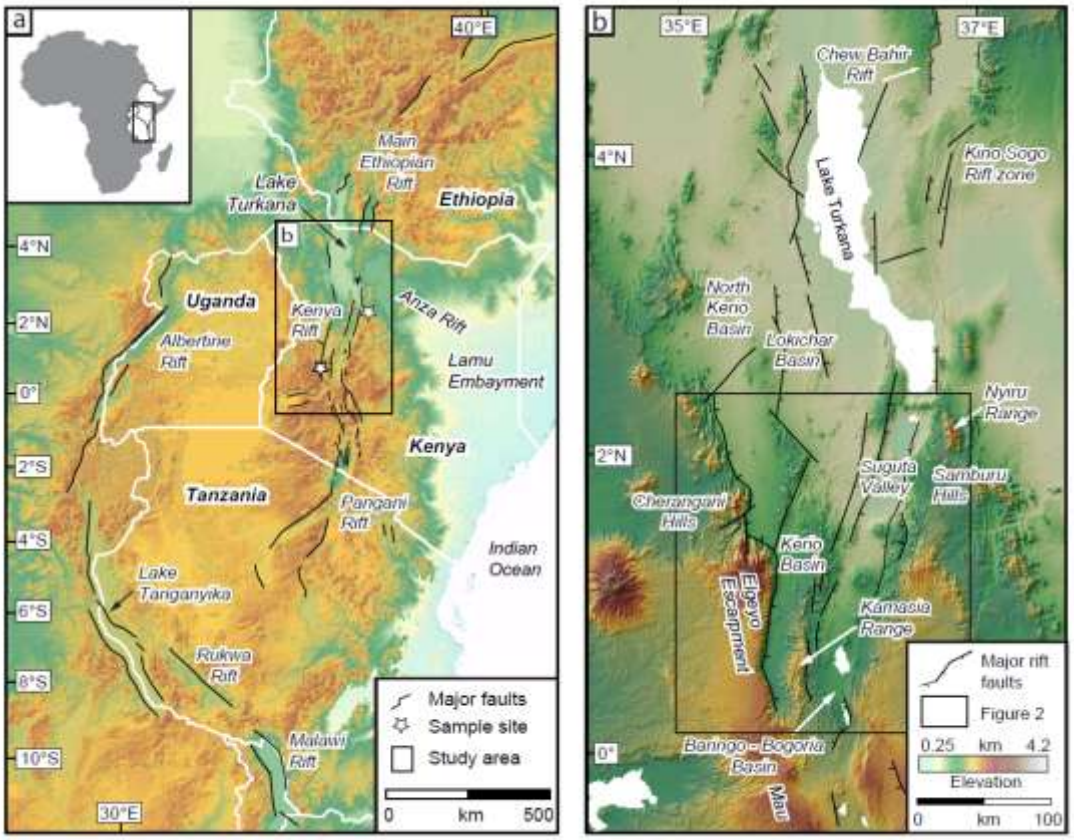

Figure 1. A. Location of the East African Rift System. Black box denotes study region in the northern and the northern sector of the central Kenya Rift. White stars denote location of sampling traverses. Grey lines denote political boundaries; B. Digital elevation model including an overview of southern Ethiopia, the northern Kenya Rift, and northernmost sectors of the central Kenya Rift.

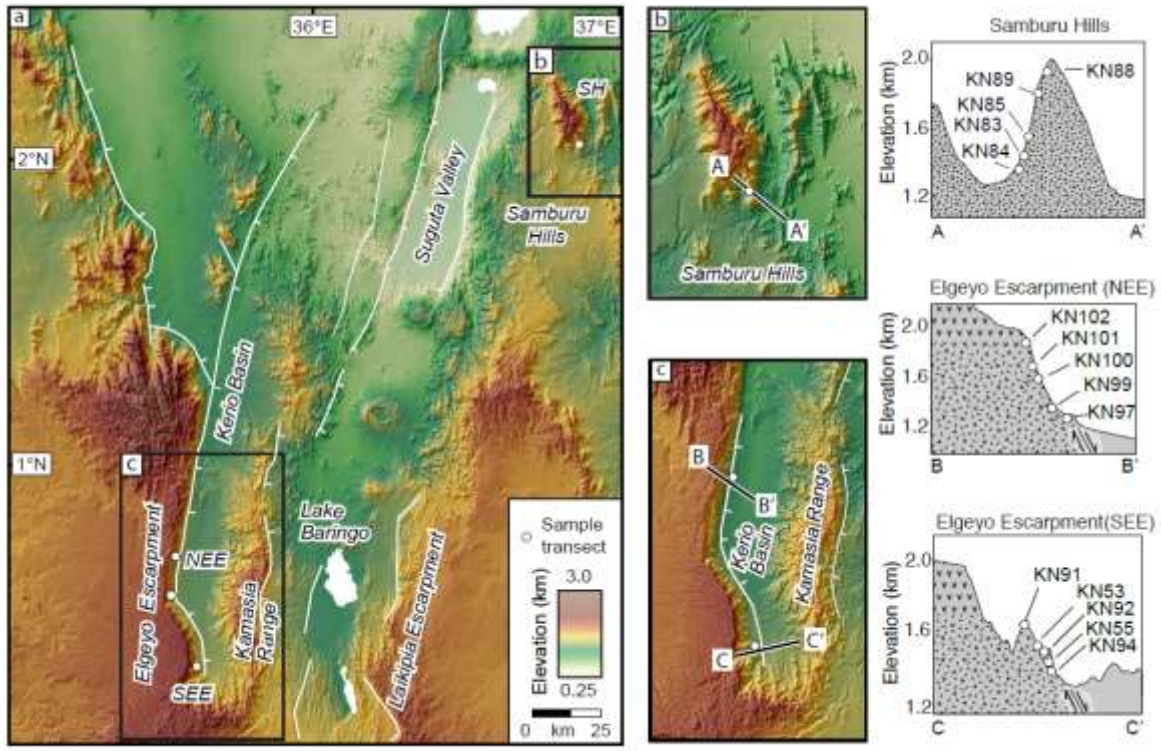

Figure 2. Digital elevation model of the study area and location and elevation of thermochronology sampling transects. Circles denote each thermochronologic sample analyzed with sample names as labels. A, study area, including Samburu Hills (SH), Northern Elgeyo Escarpment (NEE) and Southern Elgeyo Escarpment SEE); B, Samburu Hills region; C, Elgeyo Escarpment. Profiles on right show schematic elevation transects and simplified geology along the SH, NEE, and SEE sampling transects.

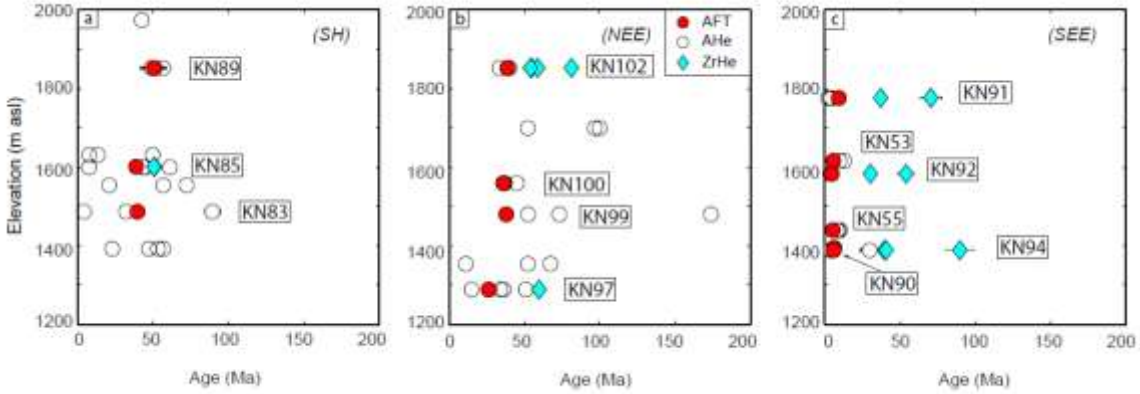

Figure 3. Age-elevation plots of the thermochronologic data. White circles denote AHe ages (not interpreted in the thermal modeling). Red circles represent AFT ages and blue diamonds denote ZHe ages; (a) Samburu Hills (SH), (b) Northern Elgeyo Escarpment (NEE), (c) Southern Elgeyo Escarpment (SEE).

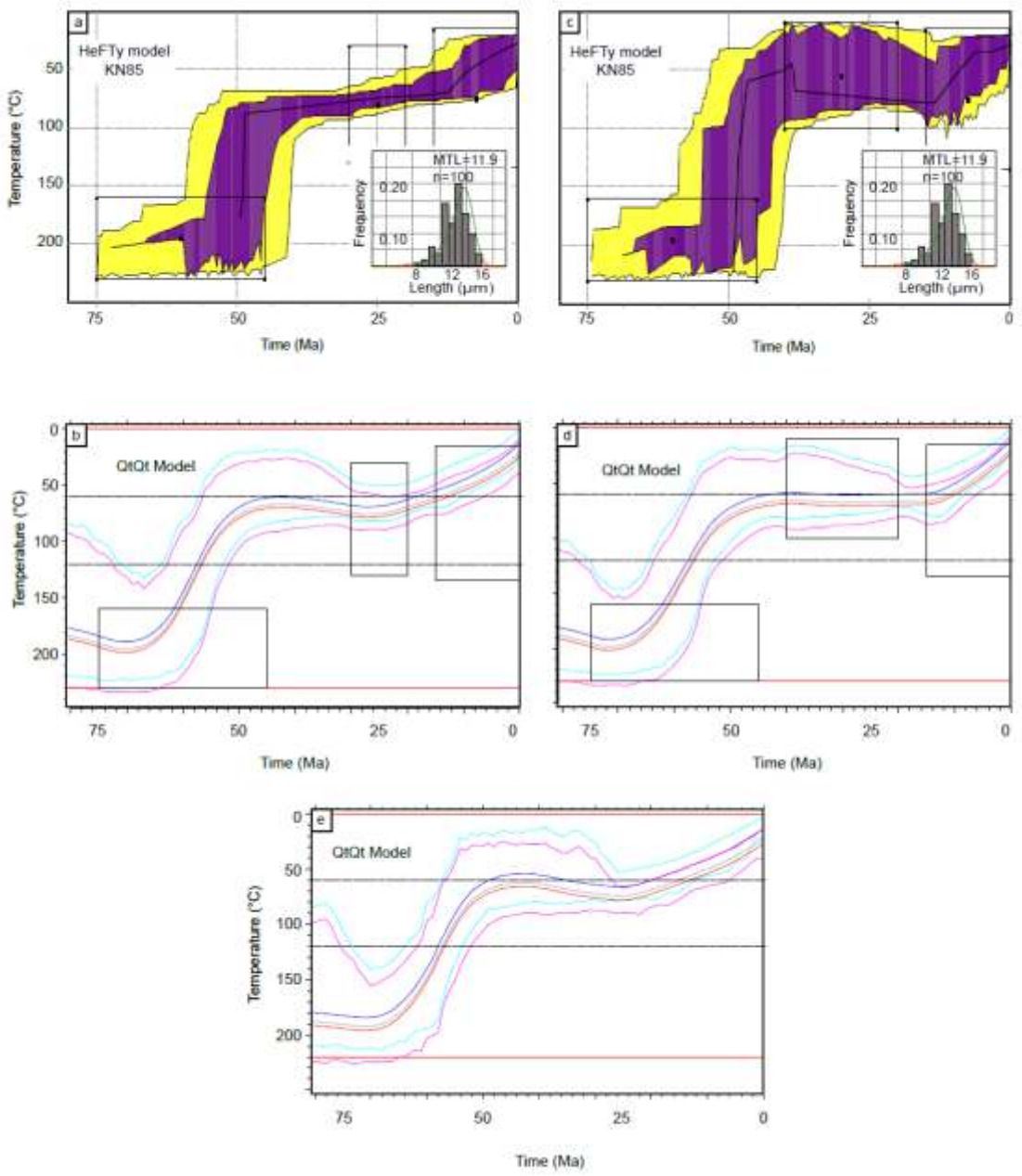

Figure 4. Thermal modeling results for the Samburu Hills (SH) samples. A and C: Time temperature model for sample KN85 from the Samburu Hills (SH) using HeFTy software [*Ketcham*, 2005] with acceptable (yellow) and good (purple) time-temperature pathway envelopes and best-fit shown with black line. The modeling scheme in A only permits monotonic cooling while C permits reheating between 40 and 20 Ma. B and D: Time-temperature histories derived from QTQt modeling, with time-temperature constraints in B

similar to those in A and with constraints in D similar to those in C. E: Time-temperature history paths derived from QTQt with no constraint boxes; red box defines the limits of the modeling, 0° - 220°C and 0-80 Ma. Blue and red lines correspond to the uppermost and lowermost sample, cyan and magenta lines correspond to 95% confidence intervals for uppermost and lowermost samples, respectively.

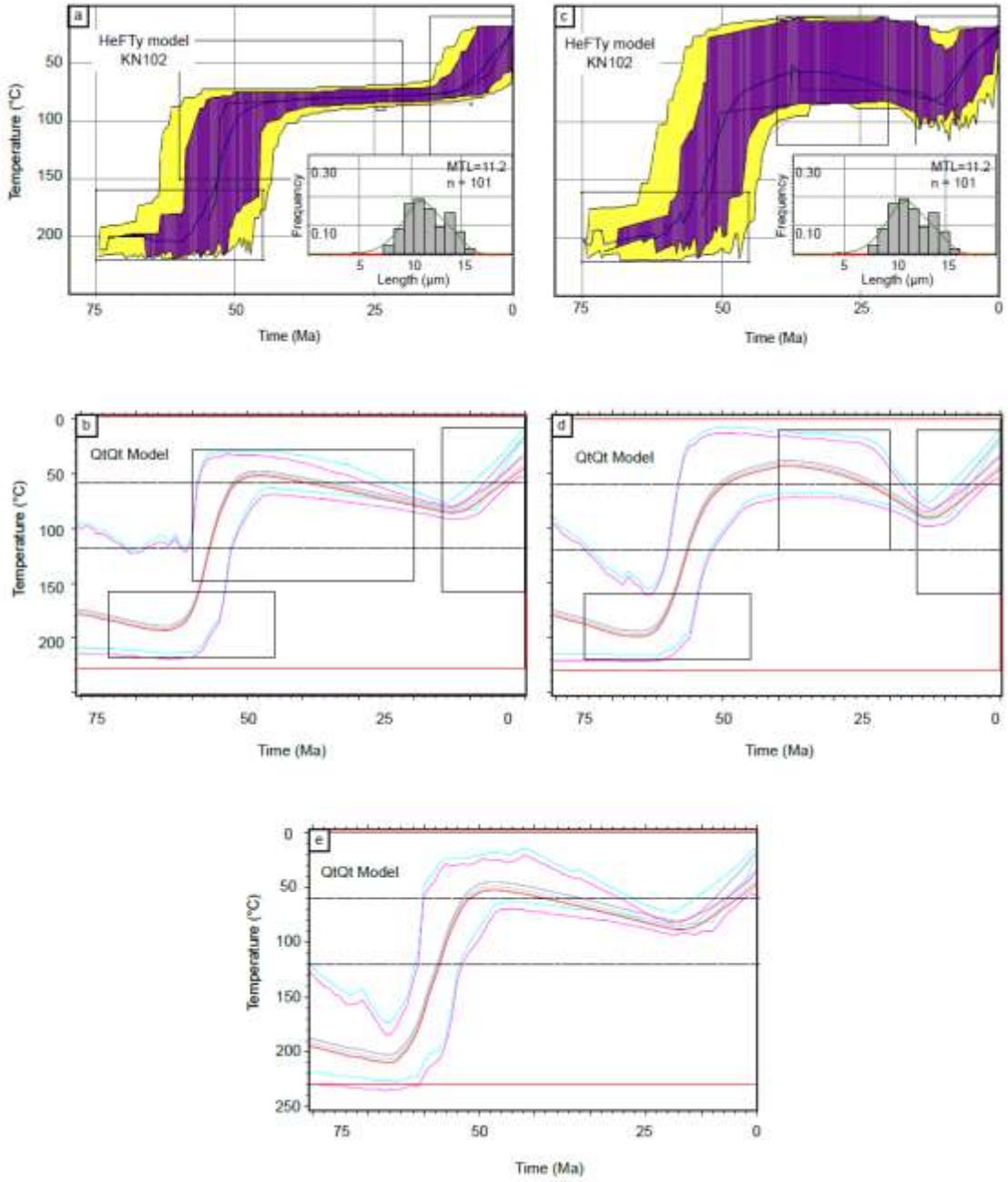

Figure 5. Thermal modeling results for the northern Elgeyo Escarpment (NEE) samples. A and C: Time temperature model for sample KN102 from the Northern Elgeyo Escarpment (NEE) using HeFTy software with acceptable (yellow) and good (purple) time-temperature pathway envelopes and best-fit shown with black line; A requires monotonic cooling while C permits reheating between 35 and 15 Ma. B and D: Time-temperature histories derived from QTQt modeling, with time-temperature constraints in B similar to those in A and with

constraints in D similar to those in C. E: time-temperature history paths derived from QTQt with no constraint boxes; red box defines the limits of the modeling, 0° - 220°C and 0 – 80 Ma.

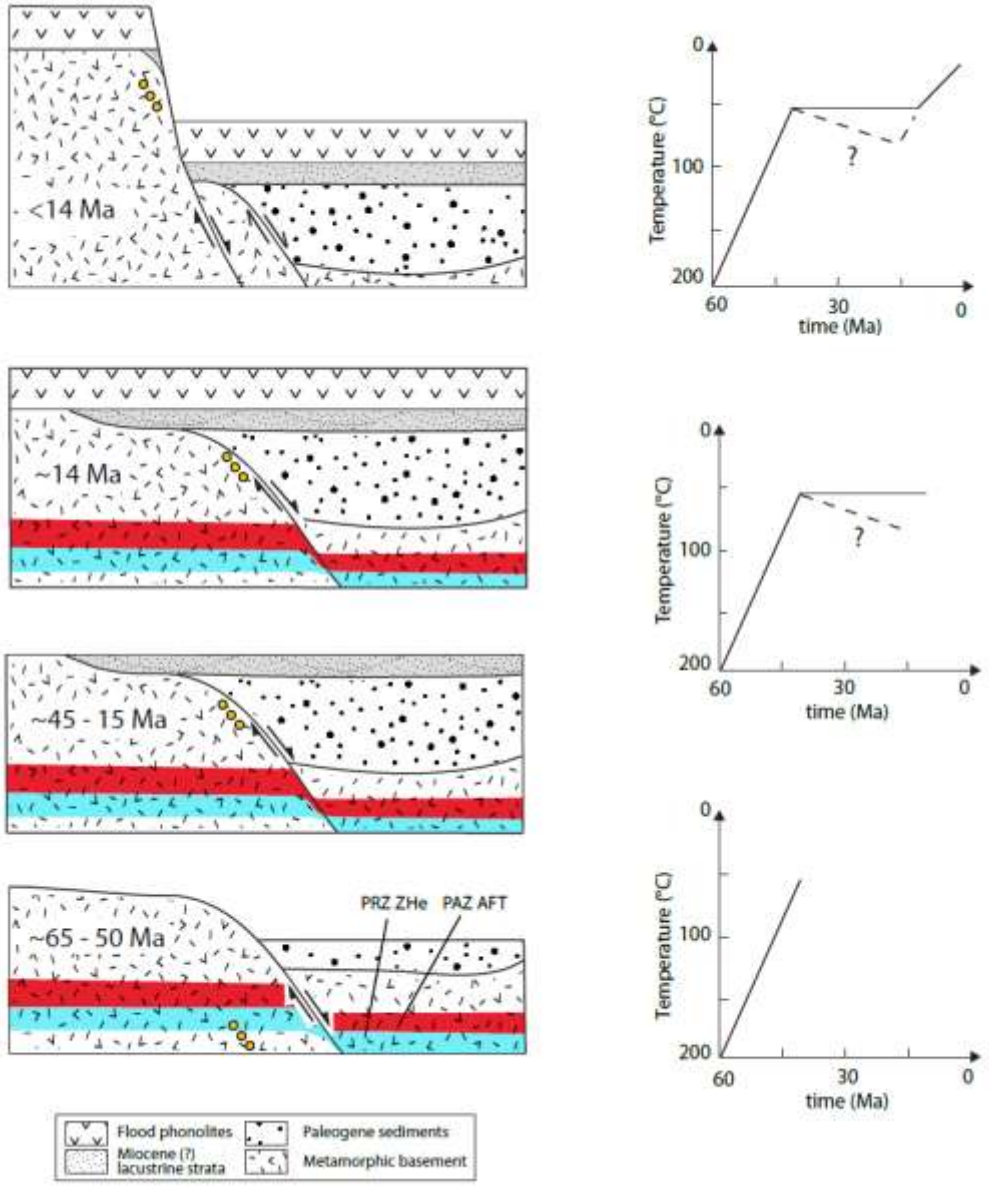

Figure 6. Cartoon of the structural and thermal evolution of the Kenya Rift along the Elgeyo Escarpment of the Kerio Valley in the transition between the central and northern Kenya rifts. Episodes of cooling occurred from ~65 to 50 Ma and from 15 to 0 Ma. Tectonic quiescence or minor reheating occurred between ~45 and 15 Ma. From bottom to top, circles denote the approximate position of the analyzed samples from ca. 50 Ma to present-day (surface). Blue band represents the inferred position of the partial retention zone for ZHe (PRZ), red band represents the apatite fission-track partial annealing zone (PAZ).

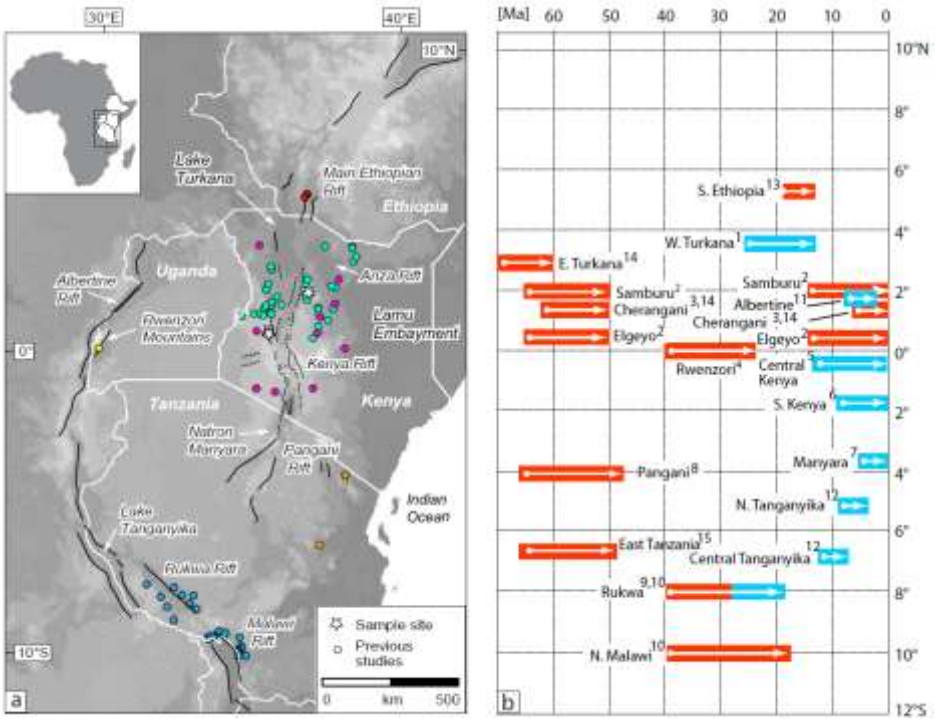

Figure 7. A. Locations of thermochronological and geological studies throughout the EARS. Thermochronological study sites are color coded: Pik et al., 2008 (red), Bauer et al., 2013 (yellow), Foster and Gleadow, 1996 and Spiegel et al., 2007 (cyan), Wagner et al., 1992 (magenta), van der Beek et al., 1998 (blue) and MBede, 2001 (orange). White outlines denote political boundaries. B. Chronogram depicting the onset of rapid cooling from thermochronology studies (red) and known extensional periods from structural constraints and basin stratigraphy (blue) in East Africa, compiled from different sources: (1) Morley et al., 1992; (2) this study; (3) Spiegel et al., 2007; (4) Bauer et al., 2013; (5) Mugisha et al., 1997; (6) Crossley, 1979; (7) Foster et al., 1997; (8) MBede, 2001; (9) Roberts et al., 2012; (10) van der Beek et al., 1998; (11) Pickford and Senut, 1994; (12) Lezzar et al., 1996; (13) Pik et al, 2008; (14) Foster and Gleadow, 1996; (15) Noble et al., 1997. Arrows indicate onset of extension, although the length of the arrows does not always reflect the full length of extensional processes at the particular location. Thermochronology study sites indicate onset of cooling inferred to represent tectonically controlled exhumation by normal faulting.